Inhibitory and disinhibitory VIP IN-mediated circuits in neocortex

Shlomo Dellal[1#], Hector Zurita[1#], Manuel Valero[1,2], Pablo Abad-Perez[1,3], Ilya Kruglikov[1], John Meng[1,4], Alvar Prönneke[1], Jessica L. Hanson[1&], Ema Mir[1], Marina Ongaro[1], Xiao-Jing Wang[1,4], György Buzsáki[1,5], Robert Machold[1], Bernardo Rudy[1,5,6*]

Affiliations:

1: Neuroscience Institute, NYU Grossman School of Medicine, New York, NY, 10016
2: Hospital del Mar Medical Research Institute, Barcelona, Spain
3: Universidad Cardenal Herrera-CEU, CEU Universities, Spain
4: Center for Neural Science, NYU, New York, NY, 10003
5: Department of Neuroscience and Physiology, NYU School of Medicine, New York, NY, 10016
6: Department of Anesthesiology, Perioperative Care and Pain Medicine, NYU School of Medicine, New York, NY, 10016

# These authors contributed equally to this manuscript

& Present address: Department of Integrative Physiology and the Institute for Behavioral Genetics, University of Colorado Boulder, Boulder, CO, 80309

* Corresponding author: Bernardo.Rudy@nyulangone.org

Abstract

Cortical GABAergic interneurons (INs) are comprised of distinct types that provide tailored inhibition to pyramidal cells (PCs) and other INs, thereby enabling precise control of cortical circuit activity. INs expressing the neuropeptide vasoactive-intestinal peptide (VIP) have attracted attention recently following the discovery that they predominantly function by inhibiting dendritic-targeting somatostatin (SST) expressing INs, thereby disinhibiting PCs. This VIP-SST disinhibitory circuit motif is observed throughout the neocortex from mice to humans, and serves as a key mechanism for top-down (feedback) and context-dependent information processing. Thus, VIP IN-mediated disinhibition has been found to play an important role in sensory processing, control of executive functions, attention, sensorimotor integration and other cortico-cortical and thalamocortical feedback interactions. Furthermore, VIP INs have been implicated in mediating the effects of reinforcement signals, both reward and aversive, via their responsiveness to neuromodulators such as acetylcholine (ACh), and in facilitating synaptic plasticity and learning. While it is evident from transcriptomic analyses that VIP INs are a molecularly heterogeneous group, the physiological significance of this diversity is unclear at present. Here, we have characterized the functional diversity of VIP INs in the primary somatosensory cortex by leveraging intersectional genetic approaches to study distinct VIP IN subtypes. We found that VIP INs can be divided into four different populations: a group that expresses the Ca^{2+}-binding protein calretinin (CR), two distinct groups that express the neuropeptide cholecystokinin (CCK), and a group that does not express either CR or CCK (non-CCK non-CR; or nCCK nCR). VIP neurons in each group exhibit different laminar distributions, axonal and dendritic arbors, intrinsic electrophysiological properties, and efferent connectivity, VIP/CR INs target almost exclusively SST INs, VIP/nCCK nCR INs also mainly target SST INs but also have connections to parvalbumin (PV) expressing INs. These two groups have essentially no connectivity to pyramidal cells (PCs). On the other hand, the two types of VIP/CCK INs target PCs, but differ in the degree to which synaptic release from each type is modulated by endocannabinoids. We also found that long-range inputs differentially recruit distinct VIP IN groups. Intriguingly, we find that distinct VIP IN populations target distinct SST INs subtypes in turn, indicating the presence of specialized VIP-SST disinhibitory subcircuits. Activation of distinct VIP IN subpopulations *in vivo* results in differential effects on the cortical network, thus providing evidence for modularity in VIP IN-mediated actions during cortical information processing.

Introduction

The remarkable diversity of GABAergic inhibitory interneurons (INs) in the cerebral cortex has been appreciated for over a century (DeFelipe, 2002; Ramón y Cajal, 1911). The specialization of INs with regard to dendritic and axonal morphology, connectivity, and intrinsic electrophysiological and synaptic properties allows for the generation of multiple distinct circuit motifs and is thereby thought to contribute to the enormous computational power of the neocortex (Fishell & Kepecs, 2020; Tremblay et al., 2016).

Recently, among the major types of INs in neocortex, the INs that express the neuropeptide vasoactive intestinal peptide (VIP) have received particular attention following the discovery that they mediate a disinhibitory circuit in multiple cortical areas. As a group, VIP INs do not provide substantial inhibition onto pyramidal cells (PCs), but instead preferentially inhibit INs expressing the neuropeptide somatostatin (SST INs), a key source of dendritic inhibition in the cortex. Several studies published in 2013-2015 reported that VIP INs in the neocortex are major targets of feedback connections and behavioral state-dependent neuromodulator release, and that their inhibition of SST INs and consequent disinhibition of PCs is a key mechanism of top-down and context-dependent processing (Fu et al., 2014; Lee et al., 2013; Pfeffer et al., 2013; Pi et al., 2013; Zhang et al., 2014). The studies were performed in L2/3, where VIP INs are enriched and are the largest IN population across different cortical areas (somatosensory barrel cortex, wS1; primary visual cortex, V1; medial prefrontal cortex, mPFC; and primary auditory cortex, A1). This work confirmed conclusions from earlier anatomical studies showing that INs expressing VIP preferentially innervated other GABAergic neurons, first performed in the hippocampus (Acsady, Gorcs, et al., 1996; Gulyas et al., 1996; Hajos et al., 1996; Kullander & Topolnik, 2021; Topolnik & Tamboli, 2022)), and suggested important roles for this disinhibitory circuit mechanism in the integration of sensory and motor signals, behavioral state-dependent control of visual responses and synaptic plasticity in V1, visual top-down attention, and in the regulation of cortical activity by reinforcement signals, respectively. Since then, numerous publications have appeared documenting the existence and functional significance of this canonical VIP-SST disinhibitory circuit, expanding the brain areas and behaviors where this motif is thought to be important. For instance, recent studies have found that VIP-dependent disinhibition is important in gating associative synaptic plasticity in olfactory cortex (Canto-Bustos et al., 2022), in goal-oriented spatial learning in the hippocampus (Turi et al., 2019), in mediat-

ing the effects of neuropeptides in the associative learning of fear memories in the auditory cortex (Melzer et al., 2021), in gating the ability of hippocampal input to generate prefrontal representations which drive avoidance behavior (Lee et al., 2019) and in sensory processing during adaptive behavior in the anterior insular cortex (Ramos-Prats et al., 2022). Underscoring their importance in cognition, VIP IN dysfunction has been implicated in schizophrenia (Batista-Brito et al., 2017; Koukouli et al., 2017), Rett syndrome (Mossner et al., 2020), and in the cognitive effects of Dravet Syndrome (Goff & Goldberg, 2019; Goff et al., 2023).

Most of these studies have treated VIP INs as a homogeneous neuronal population and relied on manipulations of total VIP INs in VIP-Cre mice. However, there is compelling evidence that VIP INs are diverse. Immunohistochemical anatomical studies in the Freund laboratory (Acsady, Arabadzisz, et al., 1996; Acsady, Gorcs, et al., 1996) provided evidence for the existence of two major types of VIP INs in the hippocampus. The majority of the VIP cells co-expressed the Ca2+ binding protein calretinin (CR or Calb2). A much smaller group co-expressed the neuropeptide CCK. Intersectional genetics based on the co-expression of VIP and CR or CCK showed that these markers also defined distinct VIP INs in the neocortex, where the VIP/CCK group is more sizable than in the hippocampus (He et al., 2016). More recently, single cell transcriptomic analyses carried out in the Allen Institute has provided evidence for extensive molecular heterogeneity of VIP INs in the neocortex (Gouwens et al., 2020; Tasic et al., 2018; Yao et al., 2021). However, the relationship between the VIP-IN molecularly defined groups and functionally-relevant categories remains to be studied and thus the physiological relevance of VIP IN diversity is not well understood at present.

Here we leveraged the accumulated transcriptomic insights with intersectional genetics to investigate the diversity of VIP INs in the neocortex. We found that VIP INs can be divided into four main populations: a group that expresses CR, two distinct groups that express CCK, and a group that does not express CR or CCK, but expresses the genes Cxcl14 and Crh. VIP neurons in each group differ in laminar distribution, morphological and electrophysiological properties and exhibit distinct connectivity patterns. VIP/CR INs almost exclusively target SST INs, whereas the non-CCK non-CR VIP INs also mainly target SST INs but also have connections to parvalbumin (PV) expressing INs. These two groups have essentially no connectivity to pyramidal cells (PCs). On the other hand, the two types of VIP/CCK INs target PCs as much or more than SST INs, but differ in synaptic properties. Notably, we find that these VIP IN populations appear to target different SST

IN subtypes, indicating the existence of several parallel VIP-SST disinhibitory circuits. Our studies also provide evidence that VIP IN subtypes are driven by different stimuli, and that activation of each VIP IN subpopulation *in vivo* has distinct effects on the cortical network. Together, our findings demonstrate the existence of multiple inhibitory and disinhibitory VIP IN-mediated circuits in the neocortex, and reveal an unexpected substructure in the regulation of information flow in the cortical network by VIP INs.

Methods

Mice

The following primary transgenic mouse lines were used to generate the compound transgenic crosses described in the present study: Vip-ires-Flpo (Jax #028578) (He et al., 2016), Cck-ires-Cre (Jax #012706), Calb2-ires-Cre (Jax #010774; CR-Cre), Crh-ires-Cre (Jax #012704), Sncg-ires-Flpo, (Jax #034424), Ai80 (Cre + Flp dependent CatCh-YFP; Jax #025109) (Daigle et al., 2018), and RC:FLTG (Flp -> tdTomato; Flp + Cre -> EGFP; Jax #026932) (Plummer et al., 2015), all obtained from the Jackson Laboratory. Additional lines included Lhx6(BAC)-EGFP (Tg(Lhx6-EGFP)BP221Gsat), ChAT-ires-Flpo (Jax #036281), and Ai80F (a Cre-deleted version of Ai80 made by us). The reporter lines Ai80 and FLTG were maintained as homozygous stocks before being crossed with compound driver lines to generate experimental animals. All experiments were conducted in accordance with protocols approved by the Division of Comparative Medicine at the NYU Grossman School of Medicine.

Histology and Immunohistochemistry

To obtain brain tissue for histological analysis, animals (P40–P60) underwent transcardial perfusion with 4% paraformaldehyde (PFA) in PBS (diluted from a 32% stock; Electron Microscopy Sciences, cat#15714). Following perfusion, brains were dissected and subjected to a post-dissection fixation period of 0–16 hours. For thin cryosection preparation, brains were equilibrated overnight in 30% sucrose/PBS, then embedded in Tissue-Plus O.C.T. compound (Scigen, cat#4583) and frozen. Cryosections (20 µm) were cut using a Leica CM3050 cryostat, mounted onto glass slides (Shandon ColorFrost Plus; ThermoScientific, cat#9991013), and stored at –20°C until further processing.

Thicker tissue sections (50-300 mm) were prepared from fixed brains in PBS using a vibratome (Leica). Some 300 µm-thick slices, initially prepared for electrophysiological recordings, were also used for histological analysis to confirm CR expression in patched neurons.

For immunohistochemistry (IHC), tissue sections were first washed in PBS, then blocked for 1 hour at room temperature in PBS containing 0.3% Triton X-100 and 2% normal donkey serum. Sections were incubated 2 days at 4°C with the primary antibody (mouse anti-CR; EMD Millipore, MAB1568; 1:1500 dilution) and 0.2% streptavidin-AlexaFluor 647 in blocking solution. Following washes in PBS, sections were incubated for 2 hours at room temperature with the secondary antibody (donkey anti-mouse AlexaFluor-488; Invitrogen, cat#A-21202; 1:1000 dilution).

Morphological analysis

Neurons were recorded using whole-cell electrophysiology while being held in an internal solution containing ~0.4% or ~1.0% biocytin for a minimum of 15 minutes. In cases where neurons were maintained for close to 15 minutes, slices were briefly returned to the incubation chamber to enhance biocytin diffusion throughout the recorded cell. After recordings, slices were fixed in 4% paraformaldehyde/PBS (prepared from a 32% stock; Electron Microscopy Sciences, cat#15714) and stored at 4°C for 1–7 days. Following fixation, slices were washed thoroughly in PBS and incubated overnight at 4°C in a 0.4% streptavidin-AlexaFluor 647 solution (Invitrogen; 498 µL 0.3% Triton X-100 in PBS and 2 µL streptavidin per slice). After incubation, slices were washed again in PBS, mounted on glass slides with Fluoromount-G (Invitrogen), and imaged using a Zeiss confocal microscope with a 40x–63x oil-immersion objective. Neuronal morphology was reconstructed in three dimensions using Neurolucida, enabling comprehensive analysis of cellular morphology.

Neurolucida Explorer was used to perform Sholl analysis on reconstructed neurons (n = 32) and to extract morphological parameters, including somatic surface area and volume, number of primary dendrites, total dendritic length, mean dendritic length, dendritic surface area, volume occupied by dendrites, dendritic polarity, total axonal length, axonal surface area, volume occupied by the axon, and axonal polarity. These parameters were subsequently analyzed using a custom MATLAB routine. Somatic localization

within cortical layers was determined by identifying either cortical columnar boundaries or layer borders, followed by quantification of the normalized position within the established limits. Layers were visually identified in confocal images based on anatomical features: (A) The L1-L2 border was defined by a sharp increase in soma density from L1. (B) The L3-L4 border was identified by the top of the barrels and the absence of pyramidal cells (PCs) characteristic of L2/3. (C) L5a appeared as a distinct band below L4. (D) The L5b-L6 border was delineated by a sharp drop in pyramidal cell density. Unbiased morphological clustering was performed using Ward's method based on all extracted morphological parameters. The Gap Statistic was used to determine the optimal number of clusters, yielding values between k=2 and k=3 across iterations. Given the stability of the clustering structure and biological interpretability, we selected k=3 with a distance threshold of 32 for final group separation. Axonal and dendritic layer distributions were quantified by dividing each vectorized reconstructed neuron into layers L1–L6. Next, vectors were isolated per layer and binarized using FIJI/ImageJ, generating a layer-dependent profile for each neuron. These profiles were further analyzed using a custom MATLAB routine

Due to their limited sample size (n=3) and clustering with VIP/SNCG neurons—the most morphologically distinct group—VIP/CCK H neurons were removed from all morphological group comparisons. To maintain biological and statistical rigor, VIP/SNCG reconstructions (n=6) were retained as a distinct alternative major group for all comparisons.

Stereotaxic injections

Both male and female mice, aged P25–P45 at the time of injection, were used in these experiments. Mice were initially anesthetized with isoflurane (~3%; 1 L/min O_2 flow for 2 minutes) before being head-fixed onto a stereotaxic frame (Kopf, Model 1900) using non-rupture ear bars. Anesthesia was maintained at 2% isoflurane throughout the procedure, and body temperature was regulated using an electronic warming pad. Under aseptic conditions, the skull was exposed, and a small craniotomy was performed over the barrel cortex (S1 BF) (coordinates: –0.90 mm AP from Bregma, ±3.20 mm ML, and 0.60 mm DV from pia) or vibrissae primary motor cortex (vM1) (coordinates: +0.80 mm AP from Bregma, ±0.25 mm ML, and 0.50 mm DV from pia) using a thin drill. Injections were delivered using a Nanoject III pressure injector (Drummond Scientific) mounted on

the stereotaxic frame. A pulled borosilicate glass injection pipette (1B100-4; World Precision Instruments) with a ~35 mm taper length and a ~40 µm tip diameter was used for precise delivery of viral preparations at a rate of 4 nL/min, with injection volumes ranging from 50–200 nL.

Slice Preparation

Adult transgenic mice of either sex (postnatal day 30–120; mean age = 44 days) were terminally anesthetized with isoflurane. Once unresponsive, mice underwent transcardial perfusion with ice-cold sucrose-based artificial cerebrospinal fluid (sucrose-ACSF) containing (in mM): 87 NaCl, 75 sucrose, 2.5 KCl, 26 $NaHCO_3$, 1.25 NaH_2PO_4, 10 glucose, 1.0 $CaCl_2$, and 2.0 $MgCl_2$, continuously saturated with 95% O_2 / 5% CO_2. Following perfusion, mice were decapitated, and the brains were rapidly extracted. The caudal portion of the brain was affixed to a slicing stage, positioning the rostral end at a 15° forward pitch. The stage was then submerged in a chamber filled with ice-cold, oxygenated sucrose-ACSF, and 300 µm-thick coronal brain sections were obtained using a Leica VT1200S vibratome. Brain slices were then incubated at 35°C for 30 minutes in either the same sucrose-based solution or the recording-ACSF (described in the electrophysiology section). Slices were subsequently maintained at room temperature for at least 1 hour before the start of electrophysiological recordings.

Electrophysiological Recordings

Brain slices were transferred to a recording chamber continuously perfused with artificial cerebrospinal fluid (ACSF) containing (in mM): 120 NaCl, 2.5 KCl, 25 $NaHCO_3$, 1.4 NaH_2PO_4, 21 glucose, 0.4 Na-ascorbate, 2 Na-pyruvate, 2 $CaCl_2$, and 1 $MgCl_2$, saturated with 95% O_2 / 5% CO_2 and maintained at 29–32°C. In select experiments, the bath solution was supplemented with the NMDA receptor antagonist D-AP5 (25 µM; Abcam) and/or the AMPA receptor antagonist CNQX (10 µM; Abcam). Neurons were visualized using differential interference contrast (DIC) optics and fluorescence illumination from an LED power source (Mightex) on an upright Olympus microscope (BX50WI or BX51WI) to identify tdTomato and/or GFP-expressing neurons. All recordings were conducted in the barrel field of the primary somatosensory cortex (S1BF), specifically in layers 2–4. Cortical layers were identified as mentioned in morphological analysis methods. Whole-cell

patch-clamp recordings were performed in current-clamp and voltage-clamp modes using an internal solution containing (in mM): 130 K-gluconate, 10 HEPES, 1.1 EGTA, 2 Mg-ATP, 0.4 Na-GTP, 10 Na-phosphocreatine, 1.5 $MgCl_2$, and 0.3–0.5% or 0.9–1.1% biocytin. The solution was adjusted to pH 7.3 using 1 M KOH. In some experiments we added a bath application of Noradrenaline (10 µM; Tocris 5169). Recording pipettes were fabricated from borosilicate glass capillaries (inner/outer diameter: 1.5 mm / 0.86 mm) using a horizontal puller (Sutter Instruments), yielding pipette resistances of 2–6 MΩ. Before obtaining whole-cell access, a gigaseal was formed, and pipette capacitance was compensated. Access resistance was monitored throughout the experiment and fully compensated; neurons with access resistances >40 MΩ were excluded from intrinsic property analyses. Electrophysiological data were acquired using a MultiClamp 700B amplifier (Molecular Devices), a Digidata digitizer (1440A or 1550B series, Molecular Devices), and Clampex software (v10.6 or v10.7, Molecular Devices). Data were sampled at 20 kHz and low-pass filtered at 10 kHz.

Electrophysiological characterization and analysis

Neurons were recorded in the VIP-Flpo; CCK-Cre; FLTG or VIP-Flpo; CR-Cre; FLTG mouse line (GFP+ somas), in the VIP-Flpo; CCKCR-Cre; FLTG cross (tdTomato+ somas), or SNCG-Flp/VIP-Cre cross to obtain the electrophysiological characterization of each VIP subclass. Neurons were characterized for intrinsic and active properties in current-clamp mode from a resting potential of ~–70 mV. Neurons were injected with 1 s long square pulses of increasing current. Parameters relating to the neuron's intrinsic and active properties were assessed as follows:

Input resistance: This was determined using Ohm's Law, based on the voltage response to a 150 ms negative current injection step, typically –20 pA.

Membrane time constant (τ): This was determined by fitting an exponential decay to the voltage response elicited by 1 s current pulses delivered at amplitudes below rheobase.

Action Potential (AP) waveform properties: To measure action potential (AP) properties, only the second AP from each sweep was analyzed, as the first AP in neurons was typically significantly faster than subsequent APs. AP threshold and peak were calculated first, with t = 0 defined at the time of the AP peak. AP threshold was defined as the

voltage at which the first derivative (dV/dt) reached 20 mV/ms. AP peak amplitude was the maximum voltage reached within 2 ms after crossing the threshold. AP half-width was the time duration during which the voltage remained above the midpoint between the AP threshold and peak. Afterhyperpolarization (AHP) was calculated as the voltage difference between the AP threshold and AP reset, where AP reset was defined as the minimum voltage recorded within a 10 ms window following the AP peak. AP max and decay slopes were the maximum and minimum values of dV/dt within 10 ms after the threshold was crossed.

All parameters were calculated for each individual AP and then averaged to obtain the mean neuronal value for each recorded cell.

Rheobase and firing rates: Rheobase was defined as the minimum current step that elicited a single AP in regular-spiking neurons or a single burst in bursting neurons. Firing rate was calculated for each voltage sweep by counting the total number of spikes within the sweep. To obtain a standardized measure across neurons, the firing rate was interpolated or taken directly at 2× rheobase.

Spike frequency adaptation*:* The adaptation index was only measured at 2 x rheobase, since near rheobase, firing was often highly irregular. The adaptation index was measured as follows: For each voltage sweep during which the neuron spiked at least six times (five ISIs), an exponential function, fadap(t), was fit to the firing-rate vs. time plot. The adaptation index (AI) for that sweep was defined as AI = fadap(1000ms) / fadap(100ms), and the values at 2 x rheobase were taken or interpolated to represent adaptation for the cell. Also measured was the area between the curves (ABC) for the fit exponential function and the line joining the initial vs ending firing rate. The firing-rate vs. time plot for SST INs is readily fit by an exponential decay whereas that for PV INs drops linearly (Meng, 2024). Thus the ABC for SST INs is non-zero whereas that for PV INs is close to zero.

Spiking regularity: For each voltage sweep, all inter-spike intervals (ISIs) from the current step were analyzed. Spiking regularity was quantified as the coefficient of variation (CV) of the ISIs, with the reported value taken from the sweeps at 2x rheobase.

VIP spiking/burst cell type classification: After determining the rheobase, additional current injection steps at rheobase intensity were applied to assess the intrinsic firing behavior of the recorded neurons. To further differentiate the electrophysiological properties among neuronal subtypes, suprarheobase current injections (1x< to 3x rheobase) were delivered. These injections provided a more detailed characterization of spike frequency adaptation, bursting propensity, and overall excitability, aiding in the classification of distinct neuronal subtypes.

Based on their responses, neurons were categorized into six distinct electrophysiological groups. 1) Burst fast adapting – Exhibited an initial high-frequency burst of at least three action potentials riding a calcium hump, followed by rapid adaptation or complete cessation of spiking at rheobase. At suprarheobase current injections, this bursting behavior was largely maintained, although some neurons generated additional action potentials following the burst. 2) Burst slow adapting – Fired an initial burst of at least two action potentials at rheobase, followed by a gradual adaptation in firing rate over the course of the current injection step at suprarheobase current injections. 3) Burst stuttering – Displayed an initial burst of at least three action potentials with fast and low afterhyperpolarizations (AHPs) at rheobase. At suprarheobase current injections, these neurons exhibited intermittent bursts of action potentials with irregular interspike intervals. 4) Non-burst adapting – Generated a single spike at rheobase and a train of spikes at suprarheobase current injections, with a gradual decrease in firing frequency over the course of the stimulus. 5) Non-burst irregular – Fired a single spike at rheobase and exhibited irregular spiking patterns at suprarheobase current injections, without a clear adaptation pattern. 6) Non-burst stuttering – Generated a single spike with fast and low AHPs at rheobase and displayed intermittent bursts of action potentials with irregular interspike intervals at suprarheobase current injections.

PV & SST IN Classifier

To test VIP output connectivity to PV and SST INs, an additional allele, Lhx6-EGFP, was introduced to label these two IN populations. In order to differentiate between the two types of INs, we used an unbiased classifier that had been trained on a set of electrophysiological data from 291 identified INs (125 PV INs and 166 SST INs). The reference cell dataset was both from this laboratory as well as from the Allen Institute. The dataset from this laboratory were all from INs in L2/3 of wS1. The viral and genetic methods

used to label reference INs included: PV-Cre;Ai9, PV-Cre + Cre-dependent virus bearing a fluorophore, the G42 and B13 GFP mouse lines, SST-Cre;Ai9, SST-Flpo + Flp-dependent virus bearing a fluorophore, SST-Cre + Cre-dependent virus bearing a fluorophore, AAV-S5E2-dTom-nlsdTom (AAV PHP.eB) (virus to label PV INs, (Vormstein-Schneider et al., 2020), AAV-S9E10-dTom (virus to label SST INs, (Furlanis et al., 2024), AAV9-Sst44-nls-mScarlet (virus to label SST INs, (Green et al., 2023; Hrvatin et al., 2019). Reference cell data from the Allen Institute were from the (Yao et al., 2021) survey, were from L2/3 of mouse primary visual cortex, and were transcriptomically identified as PV or SST INs. Electrophysiological data were fed into the Matlab Classification Learner toolbox and the following seven parameters were selected based on the feature ranking algorithm in the Matlab toolbox (see “Electrophysiological characterization and analysis” for details on how these were calculated) : Adaptation Index (AI), Adaptation Area Between Curves (ABC, see “Spike Frequency Adaptation” above), Firing rate, Membrane time constant, Input resistance, Rheobase, and AP Half-Width. Next, all classifiers in the toolbox were tested on the reference IN dataset and the Ensemble Classifier (Bagged Trees) was selected as it yielded the highest accuracy (94.2%). Next, the experimental data from Lhx6+ INs was fed into the classifier and all INs with PV scores above and below 50% were deemed, respectively, PV and SST INs.

DSI – Optogenetics

For optogenetic experiments, layer 2/3 PCs were first identified visually using DIC microscopy, then patched in whole-cell mode and confirmed as PCs through brief electrophysiological characterization. Blue light (470 nm) pulses (2 ms, >100 mA) were delivered to the slice using TTL-triggered pulses directed through a Mightex LED system under 40× magnification, with the PC soma centered in the field of view. Optically evoked inhibitory postsynaptic currents (IPSCs) were recorded under voltage-clamp mode at a holding potential of –50 mV, with D-AP5 and CNQX included in the bath solution to block glutamatergic transmission. If a connection was detected, the DSI protocol was executed as described in Figure 5.

Silicon probe implantation and recordings

Mice (n=5, 28–35 g, 3–10 months old) were implanted with 64-site silicon probes (NeuroNexus, Cambridge NeuroTech or Diagnostic Biochips) in the PPC (AP 2.0 mm, ML

1.75 mm, DL 0.6 mm), as described previously (Valero et al., 2021). Ground and reference wires were implanted in the skull above the cerebellum, and a grounded copper mesh hat was constructed, protecting, and electrically shielding, the probes. Probes were mounted on plastic microdrives that were advanced to layer 6 over the course of 5–8 d after surgery. A 100–200 µm fiber optic was attached to one of the shanks of the silicon probe. After implantation, animals were allowed to recover for at least 1 week and were housed individually under standard conditions (71–73 F and 40–50% relative humidity) in the animal facility and kept on a 12 h reverse light/dark cycle. We recorded the mice while they slept or walked around freely in the home cage, and the recording session started 1–2 hr after the onset of the dark phase.

Unit activity analysis

Spike sorting was performed semi-automatically with KiloSort 1 (https://github.com/cortex-lab/KiloSort; RRID:SCR_016422), as previously described (Valero et al., 2021) and using our own pipeline KilosortWrapper (a wrapper for KiloSort, DOI; https://github.com/brendonw1/KilosortWrapper; (Petersen et al., 2020)). This was followed by manual adjustment of the waveform clusters using the software Phy 2 (https://github.com/kwikteam/phy; (Rossant, 2021)) and plugins for phy designed in the laboratory (https://github.com/petersenpeter/phy-plugins; (Petersen, 2019)). Unit clustering generated two clearly separable groups based on their spike autocorrelograms, waveform characteristics and firing rate (Valero et al., 2021). Pyramidal cell (PC), and interneurons (INs) were tentatively separated based on these two clusters. A more reliable cell identity was assigned after inspection of all features, assisted by monosynaptic excitatory and inhibitory interactions between simultaneously recorded, well-isolated units and light responses (Valero et al., 2022; Valero et al., 2021). Units were defined as optogenetically modulated cells based on their significant modulation against randomly shuffled pulse times (500 replicates) and testing for significant difference between the observed value and the random distribution.

Statistical analysis

Statistical analyses were performed using standard MATLAB functions and GraphPad Prism. Sample size was not determined by a formal power analysis; however, the number of animals, trials, and in vitro and in vivo recorded cells were comparable to or exceeded those used in previous studies (Valero et al., 2022). All data were obtained from

experimental replicates, with a minimum of four independent experimental repeats per assay. Replication attempts were consistently successful. Data collection was not conducted under blinded conditions regarding subject groups, but data analysis was performed either blinded to the scorer or in cases where manual scoring was unnecessary. The Lilliefors test was applied to assess normality, guiding the selection of appropriate statistical tests. For normally distributed data, statistical comparisons were conducted using unpaired or paired Student's t-tests for two-group comparisons and one-way analysis of variance (ANOVA) followed by Bonferroni's post hoc test for multiple group comparisons. For non-normally distributed data or when assumptions of parametric tests were violated, statistical analyses were performed using non-parametric tests, including the two-tailed Wilcoxon paired signed-rank test for paired data, the Mann-Whitney U test for unpaired comparisons, and the Kruskal-Wallis one-way analysis of variance for multiple group comparisons. When post hoc multiple comparisons were necessary, the Dunn-Sidak correction was applied. Correlation analyses were performed using Spearman's rank correlation coefficient, with *p*-values computed via a Student's *t*-distribution applied to a transformation of the correlation coefficient. Statistical significance was defined as $p < 0.05$, with additional thresholds indicated as $p < 0.01$, $p < 0.001$, and $p < 0.0001$. For box-and-whisker plots the box represents the interquartile range (IQR: 25th to 75th percentile), the horizontal line within the box indicates the median, and whiskers extend to 1.5x the IQR unless outliers are present. Outliers are plotted individually as separate points.

Results

Heterogeneity of VIP INs in the neocortex.

VIP INs account for ~12% of the GABAergic neurons in the neocortex. They are highly enriched in superficial cortical layers, with ~60% present in L2/3, where they are the major IN population (50% of all L2/3 INs). L4, particularly its superficial part, is also enriched in VIP INs (Pronneke et al., 2015; Tremblay et al., 2016). In this study, in addition to L2/3, which has been the focus of most VIP IN studies in neocortex, we also included the cells in L4, which, as shown below resemble those in deep L2/3. VIP cells in L2-4 account for ~80% of VIP INs in the neocortex and comprise the vast majority of the VIP cells that

regulate the activity of L2/3 associative circuits. The sparse deeper layer (L5-6) VIP INs largely do not project to L2/3 and thus participate in distinct circuits (Pronneke et al., 2015).

Studies in the neocortex and the hippocampus have shown that VIP INs can be divided in two populations that differ in morphological and intrinsic electrophysiological properties based on co-expression of the neuropeptide CCK or the Ca2+-binding protein calretinin (CR) (Acsady, Arabadzisz, et al., 1996; Acsady, Gorcs, et al., 1996; He et al., 2016). In this study we first asked whether VIP/CCK and VIP/CR neurons account for all the VIP INs of the mouse barrel cortex (wS1). Comparison of the cells labeled in CR-Cre; VIP-Flp; Ai65 and CCK-Cre; VIP-Flp; Ai65 mice to the total VIP population (in VIP-Cre; Ai9 or VIP-Flp; Ai65F animals) in L2-4 of wS1 suggested there were VIP INs that were neither CR- or CCK- expressing, particularly in the middle part of L2/3. To investigate this possibility, we crossed the CR-Cre; VIP-Flp and the CCK-Cre; VIP-Flp mice to the intersectional/subtractive dual reporter FTLG (Plummer et al., 2015) (Figure 1A). With this reporter, the intersected population (containing both Cre and Flp, e.g. the VIP/CR or the VIP/CCK cells in the CR-Cre; VIP-Flp or the CCK-Cre; VIP-Flp mice, respectively) is labeled with GFP, while the remaining cells that express Flp but not Cre are labeled with tdTomato. We next generated mice with both CR-Cre and CCK-Cre paired with VIP-Flp, and crossed these animals with the FLTG reporter. This led to the discovery of a sizable population of VIP cells in L2-4 that does not express either CCK or CR (the non-CCK non-CR VIP neurons). Implementing this labeling approach allowed us to isolate, visualize and characterize this non-CCK non-CR VIP subpopulation (Figure 1B).

Differential laminar distribution and morphological properties of VIP IN populations.

The three genetically defined populations of VIP INs described above differ in their distribution within L2-4 of wS1 (Figure 1 C-F). VIP/CCK cells are most superficial, and are present in superficial L2, often near the border with L1; VIP/CR are present mainly in lower layer 2/3 and upper L4, and the non-CCK non-CR VIP neurons tend to occupy the middle part of L2/3. We performed extensive reconstructions of individual VIP INs from each of the three crosses, and found that these genetically-defined VIP IN subtypes exhibited notable differences in the morphologies of their dendritic and axonal arbors (Fig. 2), predicting subtype specificity in input and output connectivity. Most VIP INs in L2-4 have a bipolar/bitufted dendritic morphology, with 2-3 vertically oriented primary dendrites (Fig. 2;

Supplementary Figs. 2-4). The dendritic arbor of these neurons tends to be narrow and cross several layers in either direction (Fig. 2). Their ascending dendritic branch extends fully through L1, often reaching close to the pial surface. In L1, or slightly before that, the dendrite branches extensively forming a dendritic tuft, which could be target of the many cortico-cortical and subcortical projections to this layer (Schuman et al., 2021). However, some VIP/CCK cells (about a third of the sampled neurons in this group) have a multipolar dendritic morphology with dendrites extending in all directions (Fig. 2B; Supplementary Fig. 1B-C). Similarly, most of the L2-L4 VIP cells have a descending, vertically oriented and narrow axonal arbor, with branches that go deep in the column, predicting a direct influence which is vertically broad but laterally restricted. However, the axon of the multipolar VIP/CCK cells is local, largely restricted to L2/3 and is horizontally oriented, (with only a few collaterals going to deeper layers in some of the cells).

The finding of two different morphologies in the VIP/CCK group (neurons with multipolar dendritic harbor and horizontally oriented local axonal arbor (VIP/CCK H) versus neurons with a vertically oriented bipolar dendritic harbor and vertically oriented descending axonal arbor (VIP/CCK V) suggested that VIP/CCK neurons consists of two distinct populations. Interestingly, transcriptomic analysis also supports the existence of two groups of VIP/CCK INs. In addition to the IN clusters in the VIP subclass of GABAergic neurons, cells strongly expressing both VIP and CCK are found in the Synuclein γ (SNCG) IN subclass (Tasic et al., 2016; Tasic et al., 2018; Yao et al., 2021), an IN group that contains CCK basket cells (Dudok et al., 2021). To explore whether the morphological differentiation we saw within the VIP/CCK group is related to this transcriptomic differentiation, we generated Sncg-Flp; VIP-Cre mice, crossed these with the intersectional tdTomato reporter Ai65 and characterized the morphological properties of tdTomato labeled neurons. VIP/SNCG neurons were localized in superficial layer 2, near the border with L1, as observed for some of the INs labeled in the VIP/CCK intersectional mice, and resembled morphologically the multipolar VIP/CCK cells with a multipolar dendrite and horizontally oriented dendritic and axonal arbors (Fig. 2A-B; Supplementary Fig. 2 A-B). These morphological features suggest that the horizontal VIP/CCK cells likely correspond to a set of VIP- and CCK-expressing “small basket cells” (Freund et al., 1986; Kawaguchi & Kubota, 1996, 1998; Kubota, 2014; Wang et al., 2002).

While the differences in dendritic and axonal arbor between the various VIP bipolar/bitufted cells are more subtle than their differences with the multipolar VIP/CCK neurons, they might be physiologically significant. The descending dendritic process of VIP/CR neurons is longer, often reaching deeper in the column, while it is restricted mostly to L1-3 in the bipolar VIP/CCK and the VIP/non-CCK non-CR populations. The ascending dendrite of the bipolar/bitufted neurons usually finishes in a tuft which starts in L1 in VIP/CR INs and in L2 in the VIP/non-CCK non-CR population, suggesting that the two subtypes may be targeted by different sublaminar L1 inputs (Schuman et al., 2021). The axonal arbor also differs in ways that suggest differences in the postsynaptic targets of these populations. Most notably, VIP/CR cells have little axon in the upper part of L2/3 but reach deeper in the column and branch more extensively in L5 than the axon of the neurons in the non-CCK non-CR population (Figure 2; Supplementary Figures 3,4).

To independently investigate how robustly morphological differences distinguish among the genetically-defined VIP IN populations we performed unsupervised cluster analysis using Ward's method on 26 well preserved Neurolucida reconstructed VIP neurons recorded identified in the CR-Cre;VIP-Flp, the CCK-Cre;VIP-Flp and the CR-Cre;CCK-Cre;VIP-Flp; FTLG mice and 6 neurons identified in the SNCG-Flp;VIP-Cre mice. We used 16 morphological parameters: somatic surface area, volume, and location in L2/3; axonal length, surface area and volume; dendritic number, total length, mean length, surface area and volume; and dendritic and axonal x and y vectors; polarity, and sholl analysis. Unsupervised cluster analysis of neuronal morphologies confirmed the presence of four morphological groups that closely matched the molecularly/genetically defined groups (Fig. 2E). The neurons recorded in VIP/SNCG mice clustered with the multipolar neurons recorded in the VIP/CCK mice. Interestingly, as in the transcriptomic analysis, the multipolar horizontally oriented VIP neurons segregated first from all the VIP IN neurons with bipolar/bitufted morphology, including those in the VIP/CR, VIP/CCK and non-CCK non-CR VIP IN groups. The non-CCK non-CR VIP INs and the bipolar VIP/CCK INs are the most closely related groups in the cluster analysis (Fig. 2E). However, we believe they represent two distinct populations. Beyond the difference in expression of CCK in the two groups, the two show statistically significant differences in their axonal and dendritic morphology (Supplementary Figure 2, 3). Furthermore, as described below, the two populations differ in their firing patterns and connectivity.

Differential intrinsic electrophysiological properties of VIP IN subpopulations.

Cortical VIP INs have unique intrinsic electrophysiological properties that distinguishes them from other cortical INs. Most notably, VIP INs have a much higher input resistance than INs in other IN groups (345 MΩ (Pronneke et al., 2015)) compared to 69 MΩ for PV neurons (Goldberg et al., 2011), 201 MΩ for SST INs (this study); and 188 MΩ for L2/3 NGFCs (Machold et al., 2023), a property that makes VIP neurons particularly sensitive to excitatory inputs. Consistent with this, VIP INs require less current injection to reach spiking threshold (rheobase): 58.5 pA vs 257; 147; and 205 pA for L2/3 PV, SST and NGFCs, respectively. While all VIP IN subtypes had high input resistance and low rheobase, we found the input resistance was somewhat lower and the rheobase higher in VIP/CR cells (318 ± 138 MΩ and 62 ± 50 pA, mean ± SD n=56) as compared to the two types of VIP/CCK (378 ± 143 MΩ and 50 ± 25 pA and 419 ±174 MΩ and 45 ± 51 pA n=23 and 27) and the VIP/nCCK nCR neurons (378 ±155 MΩ and 45 ± 26 n=51). Interestingly, we also observed that VIP/CCK H neurons had a significantly lower spike threshold than VIP/CCK V neurons (-29 14 mv (n=23) versus -41 3 mV (n=27).

Studies of VIP INs in cortical slices have also shown that these neurons display variability in their firing patterns in response to step membrane depolarizations, and have firing patterns that are rare among INs in other IN classes, including initial bursting and irregular spiking (IS) (Lee et al., 2013; Pronneke et al., 2015; Pronneke et al., 2020). We observed similar firing patterns in our intersectional mouse lines and found that this diversity varied among the genetically defined populations (Figure 3). Bursting neurons, characterized by the presence of a depolarizing hump at subthreshold depolarizations near rheobase (likely mediated by T-type Ca2+ channels; (Pronneke et al., 2020)) and a spike burst of 2-3 spikes at >100 Hz riding on the depolarizing hump at rheobase, were much more frequently observed in the VIP/CCK populations. We distinguished three subtypes of bursting (BS) neurons: BS-strongly adapting (BS-sAD), resembled the neurons classified as fast adapting (FAD) in He et al., and Lee et al., 2010 and BS in Pronneke et al.,(Pronneke et al., 2015; Pronneke et al., 2020)). These neurons were characterized by significant failure in spiking throughout the 1sec depolarizing step during suprathreshold depolarizations. Other BS neurons had slow-adapting repetitive firing during the depolarizing step (BS-sAD). These neurons resembled the cells classified as bNA (bursting non-adapting) (He et al., 2016; Lee et al., 2013) and the cells classified as

HTBNA (high-threshold bursting non-adapting of Pronneke et al., 2015 (Pronneke et al., 2015)). A small percentage of BS neurons resembled the BS-sAD neurons but showed additional spike clusters later during the depolarizing step resulting in a stuttering pattern. All types of bursting neurons were more frequently observed in the VIP/CCK population (~ 50 % of neurons recorded in VIP/CCK mice had a bursting firing pattern). On the other hand, only 2 (out of 51) neurons recorded in VIP/CR mice showed a bursting firing pattern. The proportion of bursting neurons in the non-CCK non-CR VIP population was slightly higher (5/47).

Among non-bursting neurons we also distinguished three firing patterns. Non BS irregular spiking (non BS-IS), were characterized by the presence of intermittent action potentials elicited with irregular intervals following an initial adapting spike train at near threshold (Cauli et al., 2000; Lee et al., 2010; Porter et al., 1998). Non-BS adapting (non-BS A) resembled the cells classified as CA (continuous adapting of Pronneke et al., 2015 (Pronneke et al., 2015)). Other non-bursting neurons showed stuttering at suprathreshold depolarizations (Non-Burst stuttering). Irregular spiking and stuttering non bursting neurons were more frequently observed among the VIP/CR population, while most non-CCK non-CR neurons had a non-BS A firing pattern. Among the non-BS neurons in the VIP/CCK population we observed both non-BS A and non-BS IS neurons at a ~2:1 ratio. There was no correlation between morphological subtype of VIP/CCK neurons (multipolar or bipolar) and firing pattern, with both subtypes including both bursting and non-bursting firing patterns. Moreover, both types of firing pattern were observed in the VIP/SNCG population, which lacks the VIP/CCK bipolar subtype.

Differential output connectivity of VIP IN subtypes.

The molecular and morphological diversification of VIP INs described above would be physiologically significant if distinct VIP IN subtypes had different patterns of connectivity. There are hints that this is the case. The papers describing the CCK- and CR-expressing VIP neurons in the hippocampus suggested differential connectivity based on anatomical arguments. Most of the axonal arbor of VIP/CR cells in CA1 is located in a sublayer in the stratum oriens/alveus border which is populated by SST INs (OLM cells),

but not by PC somas or dendrites, while the axon of VIP/CCK neurons is located in stratum pyramidale, surrounding PC somata in a basket-like manner. EM studies confirmed the differential connectivity predicted by the axonal distribution (Acsady, Arabadzisz, et al., 1996; Acsady, Gorcs, et al., 1996; Gulyas et al., 1996). More recent functional studies confirmed this differential connectivity (Tyan et al., 2014). However, in the neocortex, excitatory and inhibitory cells are intermingled. Therefore, such differential connectivity is not expected based on anatomical arguments alone and would require specialized molecular mechanisms.

To study the efferent connectivity of the VIP IN populations, we expressed a channelrhodopsin (CatCh) in VIP/CR and VIP/CCK INs by crossing the intersectional mouse lines with the intersectional CatCh reporter Ai80 and used these mice to study the output connectivity of these cells to L2/3 targets in brain slices using an optogenetic approach (Lee et al., 2013). We compared the connectivity of these two IN populations to the connectivity of the total VIP IN population using VIP-Flp mice crossed to a Flp-dependent CatCh reporter derived from Ai80 to compare synaptic responses using the same opsin (see methods). The synaptic responses recorded in these studies likely arise from L2-4 VIP cells. L5-6 VIP cells only have local dendritic and axonal arbors (Pronneke et al., 2015) and are therefore unlikely to synapse on L2/3 neurons.

SST INs are relatively rare in L2/3 (12% of all INs). Therefore, to facilitate the identification of L2/3 PV and SST cells we crossed the mice to LHx6-GFP mice (Liodis et al., 2007) which labels with GFP all PV and SST cells, and used their electrophysiological features to distinguish between the two cell types using a classifier that distinguishes between these two IN types with ~95% accuracy (see Methods). Cell-type assignment of some of the recorded neurons was confirmed by comparing the dynamics of their response to local excitatory inputs, which are depressing in PV neurons and facilitating in SST neurons (Tremblay et al., 2016).

The responses observed when the total VIP IN population was stimulated in VIP-Flp mice were similar to those reported previously with VIP-Cre mice in wS1 (Lee et al., 2013) as well as in V1, auditory and prefrontal cortices (Pfeffer et al., 2013; Pi et al., 2013). Synaptic responses were largest on SST INs, and they were small but substantial on PCs and PV INs (Figure 4). In contrast, light activation of VIP/CR IN axons in CR-Cre;VIP-Flp;Ai80 mice essentially produced no synaptic responses on PCs or PV cells, but produced substantial responses on SST cells, even on SST cells recorded simultaneously

with a nearby non-responsive PC. On the other hand, light activation of VIP/CCK cell axons produced responses in PCs, comparable to those on SST cells). Like with VIP/CR INs there were negligible responses on PV cells (Figure 4). The magnitude of the synaptic responses elicited by VIP/CCK IN stimulation on PCs was similar to that elicited when the total VIP IN population was stimulated (Figure 4), suggesting that *most if not all* the connectivity of VIP INs with PCs is derived from VIP/CCK cells, and that the non-CCK non-CR VIP INs, like VIP/CR neurons, don't synapse significantly on PCs. On the other hand, the lack of connectivity of both the VIP/CCK and the VIP/CR to PV cells, suggests that this connectivity is produced by the non-CCK non-CR VIP population.

To obtain more direct information on the connectivity of the non-CCK non-CR VIP INs we searched the transcriptomic data from the Allen Institute (Yao et al., 2021) to identify genes that could be used to target this IN population. We found two genes that are expressed in non-CCK non-CR VIP INs and are not expressed in VIP/CR neurons: Cxcl14 and CRH. However, both are also expressed in some of the VIP/CCK neurons. Of the two genes, we found CRH was more useful, because it was not expressed in the VIP/CCK INs of the SNCG cluster (supplementary Figure 1). Thus intersectional VIP/CRH mice (CRH-Cre;VIP-Flp;Ai80) could we used to independently infer the connectivity of the non-CCK non-CR VIP population and to distinguish between the two VIP/CCK IN subtypes. Light stimulation of slices from CRH-Cre;VIP-Flp;Ai80 produced large synaptic responses on L2/3 SST neurons. We also observed synaptic responses in slices from these mice on PV neurons, consistent with the prediction that connectivity of VIP INs to PV INs arises from the non-CCK non-CR VIP population. We also observed responses on PCs, similar to those observed on VIP/CCK INs. We hypothesize that these synaptic responses arise from stimulation of the axons from the VIP/CCK neurons labeled in the VIP/CRH intersectional mouse line, based on our prediction that the non-CCK non-CR VIP INs have negligible connectivity to PCs (see above). Additional evidence in support of the view that the connectivity with PCs observed in the VIP/CRH line arises from the VIP/CCK neurons present in this line is presented below.

The VIP/SNCG neurons, which are excluded in the CRH-Cre;VIP/Flp intersectional mouse are also expected to synapse on PCs based on the conclusion that they correspond to the small CCK basket cells (see above). This was confirmed by light stimulation of slices from SNCG-Flp/VIP-Cre;Ai80 mice (Figure 4D). These observations suggest that the two VIP/CCK IN populations, the vertically oriented VIP/CCK V neurons and

the horizontally oriented VIP/CCK H neurons connect to L2/3 PCs. Interestingly, VIP/SNCG neurons had negligible connectivity to SST INs (Figure 4D), indicating that the connectivity to these INs in VIP/CCK mice arises entirely from the vertically oriented VIP/CCK INs

Both, the non-CCK non-CR VIP INs and the VIP/CR INs connected preferentially to SST INs, however, the synaptic responses on SST cells from non-CCK non-CR VIP cells were considerably larger than those from VIP/CR neurons (Fig. 4D). Morphological analysis showed that while non-CCK non-CR VIP INs have a high axonal density throughout L2/3, the upper part (upper 55%) of these layers is essentially devoid of axon from VIP/CR INs (Figure 2; Supplementary Fig. 2). We therefore compared the synaptic responses of L2/3 SST INs elicited by light stimulation of VIP IN axons as a function of their location in L2/3 (Fig. 4E). Consistent with the axonal distribution of VIP/CR cells, the response of SST INs located in the upper part of L2/3 to the stimulation of VIP/CR axons was significantly smaller than the response of SST INs located in the deep part of L2/3. In contrast, there was no difference in the response of superficial or deep L2/3 SST INs to stimulation of VIP/CRH axons. Stimulation of VIP/CCK axons produced essentially no response on the most superficial SST INs (0-30 % of L2/3) but produced similar responses on SST neurons located between 30-55 and 55-100% of L2/3. This finding is consistent with the observation that the horizontal VIP/CCK neurons (VIP/SNCG) which dominate the VIP/CCK cells in the most superficial part of L2/3 have no connectivity to SST INs (Figure 4).

Differential synaptic properties of the two VIP/CCK IN populations.

We screened the transcriptomics database (Allen Institute scRNAseq data; (Yao et al., 2021)) for molecular differences between the two types of VIP/CCK INs and found that they differ in terms of expression of CB1 endocannabinoid receptors, which are highly enriched in the multipolar/horizontal SNCG/VIP neurons as compared to the bipolar/vertical VIP/CCK V cells (Fig. 5A). We investigated whether this resulted in differences in synaptic connections to PCs. Endocannabinoids are known to mediate a phenomenon known as depolarization induced suppression of inhibition (DSI; (Pitler & Alger, 1992; Wagner & Alger, 1996), which has been observed on the synaptic connections of CCK BCs (Bodor et al., 2005; Galarreta et al., 2008). Depolarization of a connected pyramidal cell leads to the release of endocannabinoids from the pyramidal cell that then bind to CB1 receptors

located on the presynaptic terminals of the CCK BCs, leading to suppression of GABA release (Ohno-Shosaku et al., 2001; Wilson et al., 2001; Wilson & Nicoll, 2001). Consistent with the difference in their levels of expression of CB1 receptors, we observed a much stronger DSI on the synaptic responses elicited by light stimulation of the VIP/CCK H INs in the VIP/SNCG mouse as compared to light stimulation of the VIP/CCK V INs and the non-CCK non-CR VIP neurons in the VIP/CRH mouse (Fig. 5B & C). The DSI of the responses elicited on VIP/CCK mice, in which all VIP/CCK INs are stimulated, was intermediary, between to those observed on VIP/SNCG and VIP/CRH mice (Fig. 5C). This result supports the conclusion that both types of VIP/CCK INs target PCs.

Differential input connectivity of VIP IN subtypes.

The studies of efferent connectivity show that distinct VIP IN subtypes differ in their postsynaptic targets. This would be highly significant if these populations were driven by distinct excitatory sources, implying that different behavioral contingencies recruit distinct VIP IN subtypes and thereby inhibit or disinhibit PCs, or inhibit different subtypes of SST INs and thereby disinhibit distinct types of PCs. We therefore next investigated the input connectivity of the VIP IN populations. Of the three major long-range inputs to wS1: vibrissa motor cortex (vM1), secondary somatosensory cortex (S2) and the somatosensory higher-order thalamic nucleus POm, the inputs from vM1, which are thought to mediate sensorimotor integration in the whisker system, have been shown to preferentially target VIP INs in L2/3 (Lee et al., 2013; Naskar et al., 2021). To explore the connectivity of vM1 inputs to distinct VIP IN subtypes in wS1, we virally expressed ChR2 in vM1 excitatory neurons (Lee et al., 2013) and recorded postsynaptic responses to light stimulation of identified VIP IN populations in L2-4 of wS1 (Fig. 6). All VIP IN subtypes responded to light stimulation of vM1 afferents, but the response was significantly larger on the non-CCK non-CR VIP population, as compared to the VIP/CCK V and VIP/CR populations, and often led to action potential firing when recorded under current clamp (Figure 6).

VIP INs are also strongly stimulated by cholinergic stimulation, likely mediated by $\alpha4\beta2$ nicotinic receptors (Askew et al., 2019). Stimulation of ChAT cells or arousal produces much larger non-glutamatergic excitation of VIP INs than any other cells in L2/3 (Figs. 1E, 3C in (Gasselin et al., 2021)), but the responses of individual cells are very variable. This variability may arise from differential targeting of VIP IN subtypes by cholinergic inputs. Transcriptomic analysis shows that all VIP IN populations express several nicotinic receptor alpha subunits, with $\alpha4$ being the dominant subtype (Fig. 6). The levels

of α4 transcripts were lower in the non-CR/non-CCK VIP INs as compared to VIP/CCK and VIP/CR subtypes (Fig. 6G). Consistent with this pattern, the responses elicited by light stimulation of ChR2-expressing cholinergic axons were lower in the non-CR/non-CCK VIP INs than those recorded on L2/3 VIP/CCK or VIP/CR neurons (Fig. 6).

Transcriptomic analysis (Yao et al., 2021) also shows differential expression of α1a and α1b adrenergic receptors on VIP IN subtypes (Fig. 6L). Transcriptomic subtypes that correspond to VIP/CCK INs strongly express α1b receptors, while those that correspond to the non-CCK non-CR VIP population express both α1a and α1a. Adrenergic receptors were weakly expressed in VIP/CR INs. We compared the effect of bath application of the adrenergic agonist noradrenaline (10 μM) on VIP/CR, VIP/CCK and VIP/non-CCK non-CR neurons. Consistent with predictions based on transcriptomic analysis responses were significantly smaller on VIP/CR cells compared to those on the VIP/CCK and VIP/non-CCK non-CR populations (Figure 6N).

Monosynaptic rabies tracing could be a useful approach to discover additional sources of excitation for specific VIP IN subtypes. This will be facilitated when tools for intersectional rabies tracing, currently under development, become available.

VIP IN-mediated inhibition and disinhibition in neocortex.

The connectivity data suggest that while the activity of VIP/CR INs is likely to produce disinhibition of PCs, activity in VIP/CCK cells might inhibit PCs, since their relatively weaker connection to INs might not be sufficient to produce disinhibition. In fact, most INs connect to other INs (Pfeffer et al., 2013; Tremblay et al., 2016). To produce disinhibition of PCs, the reduced inhibition from SST cells has to be able to overcome the inhibition the PCs receive directly from the VIP/CCK cells or other INs active in the same context.

We used silicon probes to record the effects of optogenetic stimulation of VIP/CR or VIP/CCK INs on the activity of PCs in posterior parietal cortex (PTLp) in freely moving mice. We used the intersectional VIP/CR and VIP/CCK mice crossed to the intersectional channelrohodopsin reporter mouse Ai80. Light stimulation of VIP/CR INs *increased* the activity of a fraction of the recorded PCs, and inhibited a population of INs, presumably SST cells (Figure 7). On the other hand, light stimulation of VIP/CCK INs inhibited a fraction of the recorded PCs (as well as some INs) (Figure 7). The observed effect is likely an underestimate of the inhibition of PCs by VIP/CCK INs, since silicon probe recordings are biased against superficial layers (Machold et al., 2023; Senzai et al., 2019), where the

axon of VIP/CCK cells is concentrated. These results support the hypothesis that VIP/CR INs are disinhibitory while VIP/CCK neurons are inhibitory as predicted by the connectivity studies in slices.

Discussion

The development and introduction of genetic methods in rodents to label and manipulate the major IN subclasses in cortex (PV, SST, VIP and ID2 or Lamp5) have been transformative, and have resulted in major advances in our understanding of cortical circuits (Machold & Rudy, 2024; Taniguchi et al., 2011). It is now evident that these IN groups are heterogeneous and are comprised of discrete subtypes that often have functionally important differences in connectivity and function. For example, PV INs encompass both basket cells and chandelier cells, populations that share similarities in molecular gene expression and intrinsic electrophysiological properties but that have very different output connectivity: basket cell terminals target the soma and proximal dendrite of PCs whereas axo-axonic cells target the PC axon initial segment. Recent work has underscored the importance of this next level of organization, as illustrated by the monumental single-cell transcriptomic analyses of cortical neuron types by the Allen Institute (Gouwens et al., 2020; Tasic et al., 2016; Tasic et al., 2018; Yao et al., 2021), the analysis of the diversity of PV basket cells (Gouwens et al., 2020), of chandelier cells (Wang et al., 2019), and of SST INs (Hostetler et al., 2023; Ma et al., 2006; Muñoz et al., 2017; Nigro et al., 2018; Wu et al., 2023). Considering that no single non-overlapping set of genes have been identified for the vast majority of IN subtypes, progress in understanding the functional specialization of IN subpopulations has relied on the development of new approaches that give experimental access to this diversity in a practical reasonable way. In this study we applied intersectional genetic methods to reveal clearly distinct functional populations of VIP INs.

We found that VIP INs can be subdivided into four main groups that exhibit distinct laminar organization, stereotypical patterns of axonal and dendritic arborization and differences in input and output connectivity. The two types of VIP/CCK INs, which account for about 30% of L2-4 VIP neurons both provide inhibition onto PCs (Figure 4), but had interesting differences in their synaptic properties (Figure 5). They are predicted to mediate inhibition on PCs while the VIP/CR cells and the non-CCK non-CR VIP INs predominantly target SST INs and are predicted to be disinhibitory (Fig. 4). *In vivo* experiments

exploring the effect on the cortical network of light stimulation of ChR2 expressing VIP/CCK or VIP/CR neuron subtypes in freely moving mice provided validation of these predictions (Figure 7).

Interestingly although both the VIP/CR and the non-CCK non-CR VIP INs predominantly target SST INs, we found that they differed in the populations of L2/3 SST INs that receive strong innervation from each subtype. VIP/CR INs mainly target SST INs in deep L2/3, while the non-CCK non-CR VIP INs equally targeted superficial and deep L2/3 SST INs (Figure 4). Distinct SST IN subtypes, with different localization in the cortical column have been shown to inhibit different types of PCs and/or different compartments of the same PC (Wu et al., 2023). This predicts that distinct VIP IN subtypes may disinhibit distinct subsets of PCs. Moreover, we found that non-CCK non-CR VIP neurons but not VIP/CR cells also target PV INs, albeit much less than SST INs, suggesting that inputs targeting these VIP INs produce disinhibition of both the soma and the distal dendrite of PCs, and thus could facilitate both feedforward and feedback inputs.

Examination of the inputs to VIP INs in wS1 by long-range projections also indicated that there is differential targeting of VIP subtypes. Glutamatergic inputs from vM1 preferentially targeted non-CCK non-CR VIP INs, whereas these VIP neurons received the weakest input from cholinergic axons from the basal forebrain (Fig 6). Lastly, we found strong noradrenergic responses on both VIP/CCK and non-CCK non-CR VIP INs but not on VIP/CR cells. Given their differential efferent connectivity, this indicates that the functional effect of any stimulus that activates VIP INs depends on which VIP IN subpopulations are targeted. Together, the results suggest that VIP IN subtypes form highly specific circuits, as has been proposed for SST IN subtypes (Wu et al., 2023).

L2-4 VIP INs project a significant amount of axon to deep cortical layers (Figure 2 and Supplementary Figs), where a diverse population of SST INs reside (Hostetler et al., 2023; Ma et al., 2006; Muñoz et al., 2017; Nigro et al., 2018; Tremblay et al., 2016; Wu et al., 2023). Furthermore, paired recordings have shown that L2/3 VIP cells strongly connect to deep layer SST cells (Jiang et al., 2015; Jiang et al., 2013; Pfeffer et al., 2013). It will be of great interest to investigate whether L2-4 VIP/CR and non-CCK non-CR VIP INs differentially target distinct L5-6 SST subpopulations. This requires the development of methods to identify specific SST subtypes that are compatible with the genetics used to select distinct VIP IN subtypes for stimulation. The recent discovery of enhancers labeling specific SST IN subpopulations is promising in this regard (Hrvatin et al., 2019). These

studies will also require the ability to express optogenetic actuators independently in superficial versus deep VIP INs.

The VIP-SST disinhibitory circuit motif has emerged as a key circuit mechanism for top-down modulation and context-dependent cortical processing (see recent reviews by (Apicella & Marchionni, 2022; Fu et al., 2015; Gentet et al., 2012; Gonchar & Burkhalter, 2003; Lee et al., 2013; Letzkus et al., 2015; Letzkus et al., 2011; Sachidhanandam et al., 2016; Topolnik & Tamboli, 2022; Tremblay et al., 2016; Williams & Holtmaat, 2019). The existence of VIP IN subtypes with different output connectivity may explain some results that appear to contradict the view that increased activity of VIP neurons produces disinhibition of excitatory neurons. For instance, while in V1, locomotion increases sensory responses (Fu et al., 2015), in auditory cortex (A1) it does the opposite, although in both cases VIP INs are recruited. The VIP disinhibitory circuit has been implicated as the cause of increased responses in V1 (Fu et al., 2015). A recent study, while confirming that movement suppresses responses in auditory cortex, shows that in contrast, optogenetic activation of VIP INs in this cortical area also increases stimulus-evoked spike rates (Bigelow et al., 2019). One possibility is that while activating VIP INs optogenetically excites all VIP subtypes, in A1 movement might preferentially recruit inhibitory VIP/CCK cells. In another example Batista-Brito (2017) (Batista-Brito et al., 2017) showed that deletion of the schizophrenia-related gene ErbB4 specifically from VIP INs impaired VIP IN function and produced dramatic effects on visual responses and severe deficits in cortical activity, visual responses, sensory perceptual function and other behavioral changes characteristic of models of schizophrenia. However, deletion of ErbB4 from VIP-INs also led to a marked increase in the activity of cortical excitatory neurons. One possibility is that ErbB4 deletion in VIP cells primarily affected VIP/CCK INs, and that it is the impairment of VIP IN-mediated inhibition that is responsible for the effects. Overall, it is increasingly clear that the heterogeneity of VIP INs observed in molecular profiling and electrophysiological studies is functionally important, and provides additional flexibility and modularity to disinhibitory circuitry in the brain.

Figure 1: VIP subtypes

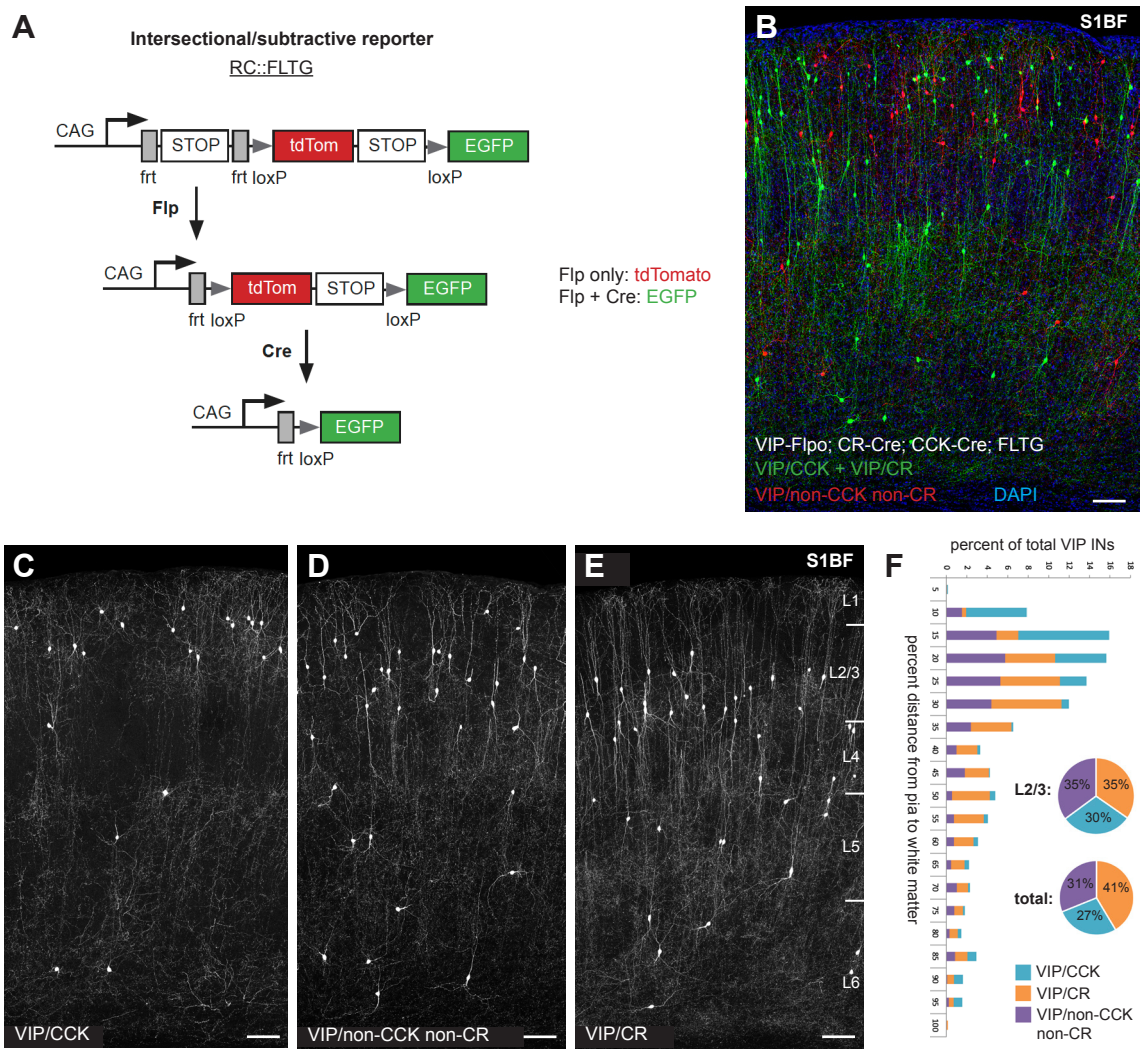

Figure 1 Dissection of VIP IN populations using intersectional genetics

(**A**) Schematic of the FLTG reporter. Flp activity results in tdTomato expression and Flp + Cre results in EGFP expression. (**B**) Image of a brain tissue section (wS1) from VIP-Flpo; CR-Cre; CCK-Cre; FLTG animals illustrates the VIP/nonCR non-CCK population (red). (**C-E**) Images of VIP/CCK (**C**), VIP/nonCCK nonCR (**D**) and VIP/CR INs labeled using the FLTG reporter (50 μm thick sections of wS1 cortex). (**F**) Graphical representation of the proportions of each VIP subtype shown in C-E from the pia to white matter in 5% increments. Pie charts summarize the overall proportions of each subtype in L2/3 and overall (wS1). Scale bars in B-E represent 100 μm.

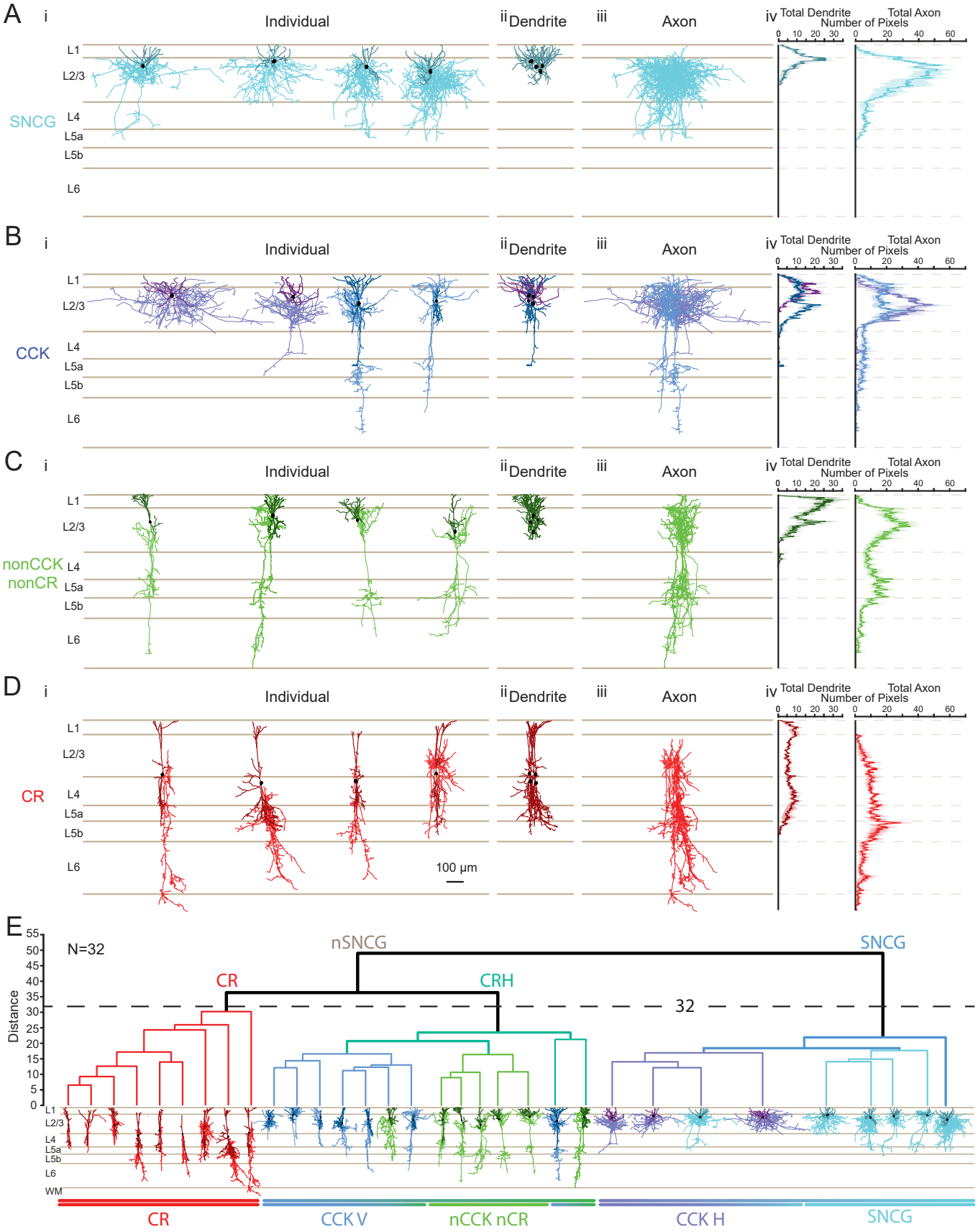

Figure 2. Morphological Characteristics of VIP IN populations.

(A)VIP/SNCG-expressing neurons. **(i)** Complete Neurolucida reconstructions of four biocytin-filled neurons in VIP-Cre/SNCG-Flp mice, showing the distribution of dendrites (dark cyan), axons (light cyan), and soma (black) across cortical layers. **(ii)** Superimposed dendrites and somata of the four neurons. **(iii)** Superimposed axons of the four neurons. **(iv)** Quantification of pixel distribution across the cortical column for total reconstructed dendrites (left) and axons (right). **(B)** Same as **(A)** for four CCK-expressing neurons reconstructed from VIP-Flp/CCK-Cre/FLTG mice. CCK+ neurons were classified as CCK Horizontal (CCK H) and CCK Vertical (CCK V), with their respective dendrites (dark lavender for CCK H, dark blue for CCK V), axons (light lavender for CCK H, light blue for CCK V), and soma (black). Quantification of pixel distribution for total reconstructed dendrites (left) and axons (right) in **(iv)** is shown for CCK H and CCK V neurons. **(C)** Same as **(A)** for non-CCK, non-CR VIP neurons reconstructed from VIP-Flp/CCKCR-Cre/FLTG mice, with dendrites shown in dark green, axons in light green, and soma in black. **(D)** Same as **(A)** for CR-expressing neurons reconstructed from VIP-Flp/CR-Cre/FLTG mice with dendrites shown in dark red, axons shown in light red, and soma in black. **(E)** Unbiased hierarchical clustering (Ward's method) was performed on all reconstructed neurons (n = 32) using a comprehensive set of morphological parameters, including somatic localization, surface area, volume, number of primary dendrites, total dendritic length, mean dendritic length, dendritic surface area, dendritic volume, dendritic polarity, total axonal length, axonal surface area, axonal volume, and axonal polarity. The Gap Statistic was used to determine the optimal number of clusters, leading to the selection of a distance threshold of 32 for final group separation. The most pronounced morphological distinction was observed between VIP/SNCG-like and VIP/non SNCG neurons, followed by the separation of VIP/CR and VIP/CRH-like neuronal morphologies. Below the clustering dendrogram, each corresponding morphology is displayed for visualization.

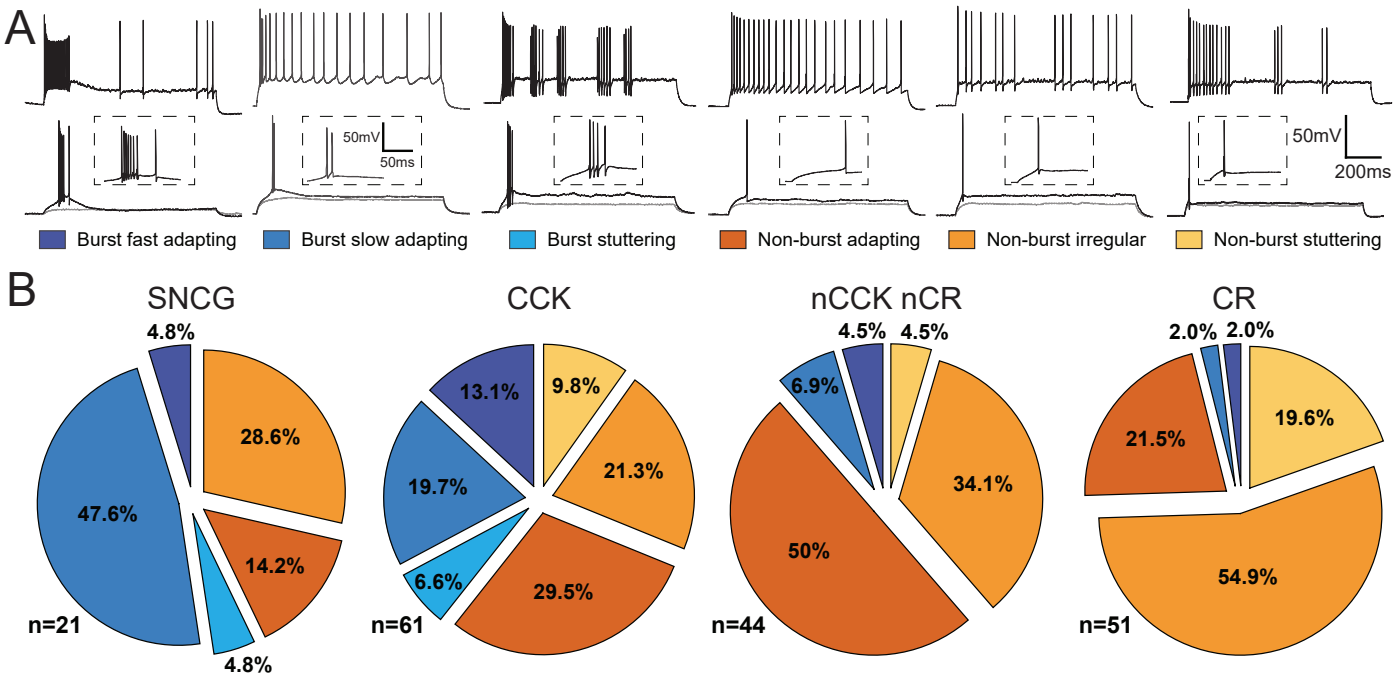

Figure 3 Firing patterns of VIP IN populations.

(A) Firing properties of VIP INs in response to step depolarizations. Shown are the responses of representative cells to a just subthreshold, threshold, and suprathreshold current injection. Insets show a magnification of the area near the first spike for the threshold response. L2-4 VIP neurons in wS1 showed one of six distinct firing patterns: Burst fast adapting (dark blue) neurons exhibited an initial high-frequency burst of at least three action potentials riding on a calcium hump (inset), followed by rapid adaptation or complete cessation of spiking at rheobase (bottom). During suprathreshold current (top) injections, these neurons largely maintained bursting behavior, though some generated additional spikes. Burst slow adapting (medium blue) neurons fired an initial burst of at least two action potentials at rheobase (bottom; inset), followed by a gradual adaptation in firing rate over the duration of the current injection step at suprathreshold levels (top). Burst stuttering (light blue/cyan) neurons displayed an initial burst of at least three action potentials with fast and low afterhyperpolarizations (AHPs) at rheobase (bottom; inset). During suprathreshold depolarizations, these neurons exhibited intermittent bursts of action potentials with irregular interspike intervals (top). Non-burst adapting neurons (dark orange) generated a single spike at rheobase (bottom; inset) and a train of spikes during suprathreshold current injections, showing a gradual decrease in firing frequency over the course of the depolarizing step (top). Non-burst irregular neurons (medium orange) fired a single spike at rheobase (bottom; inset) and exhibited irregular spiking patterns at suprathreshold depolarization, without a clear adaptation pattern (top). Non-burst stuttering (light orange/yellow) neurons generated a single spike with fast and low AHPs at rheobase (bottom; inset) and displayed intermittent bursts of action potentials with irregular interspike intervals during suprathreshold current injections (top). **(B)** Electrophysiological Subtype Distribution of firing patterns in VIP IN populations. Shown is the proportion of distinct firing patterns for VIP/SNCG (n = 21), VIP/CCK (n = 61), VIP/nonCCK/nonCR (n = 44), and VIP/CR (n = 51) neurons. VIP/SNCG and VIP/CCK neurons predominantly exhibited bursting firing patterns, whereas VIP/nonCCK/nonCR neurons were more commonly associated with non-burst adapting behavior, and CR neurons displayed a higher prevalence of irregular spiking phenotypes.

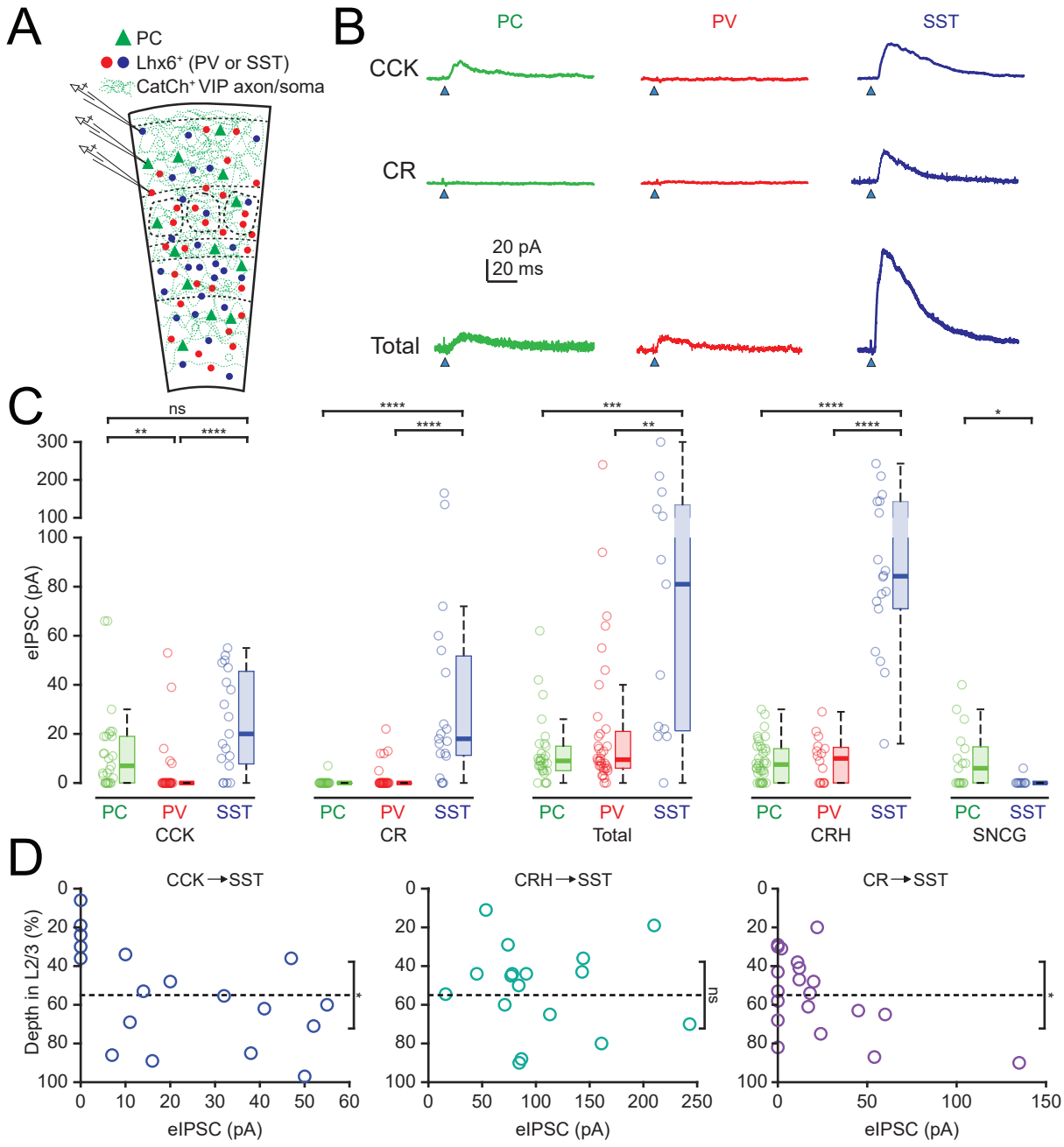

Figure 4 Efferent connectivity of VIP IN populations.

(A) Schematic of the experiments to study efferent connectivity of VIP IN populations using Ai80 mice. Either PCs or EGFP+ Lhx6+ INs (PV or SST cells) in wS1 were patched to measure output from VIP INs following light stimulation of CatCh-expressing VIP IN axons. **(B)** Representative voltage-clamp (Vhold = -50 mV) recordings of evoked VIP IN output to PCs, PV or SST INs. An unbiased classifier (see Methods) was used to differentiate between PV and SST INs among Lhx6+ neurons. The top, middle, and bottom rows were from representative neurons in the VIP;CCK;Ai80;Lhx6-EGFP, VIP;CR;Ai80;Lhx6-EGFP, and VIP;Ai80-frt;Lhx6-EGFP mouse lines, respectively. **(C)** Quantification of evoked inhibitory postsynaptic currents (eIPSCs) in PCs, PV INs, and SST INs following light stimulation of VIP/CCK, VIP/CR, Total VIP, VIP/CRH and VIP/SNCG IN axons. Box-and-whisker plots. The box represents the interquartile range (IQR: 25th to 75th percentile), the horizontal line within the box indicates the median, and whiskers extend to 1.5x the IQR unless outliers are present. Outliers are plotted individually as separate points. (n, respectively, for PC, PV, SST: in VIP/CCK (27,30,19), in VIP/CR (22,31,19), Total (30,36,13), VIP/CRH (38,16,18), VIP/SNCG (17 PC, 10 SST), Kruskal-Wallis test followed by a Dunn-Sidak post hoc test: CCK, $p<0.0001$, PC vs PV $p=0.00371$, PC vs SST $p=0.32007$, PV vs SST $p=1.97\times10^{-5}$; CR, $p<0.0001$, PC vs PV $p=0.79165$, PC vs SST $p=3.42\times10^{-8}$, PV vs SST $p=2.74\times10^{-7}$; Total, $p=0.0003$, PC vs PV $p=0.69629$, PC vs SST $p=0.000203$, PV vs SST $p=0.002501$; CRH, $p<0.0001$, PC vs PV $p=0.99948$, PC vs SST $p=7.87\times10^{-9}$, PV vs SST $p=3.34\times10^{-6}$; SNCG, PC vs. SST, Mann-Whitney test, $p=0.0204$). **(D)** Quantification of evoked inhibitory postsynaptic currents (eIPSCs) from VIP/CCK, VIP/CRH, and VIP/CR output to L2/3 SST INs by depth in L2/3, with the L1/2 and L3/4 borders being 0% and 100%, respectively. The dashed line indicates the 55% depth mark which is the cutoff for high and low VIP/CR axon density (Figure 2, and supplementary Fig. 2). For VIP/CR INs the eIPSC amplitudes in SST INs below this cutoff are significantly larger on average than those above the cutoff (right panel, Two-sample t-test, $p=0.0477$). In contrast, eIPSC amplitudes on SST INs evoked from VIP/CRH INs are not significantly different between the two regions (middle panel, Two-sample t-test, $p=0.2655$). eIPSC amplitudes evoked on SST INs from VIP/CCK INs are also significantly higher in the bottom vs top region (left panel, Two-sample t-test, and near zero in the top 30% of L2/3, which may reflect the fact that VIP/SNCG neurons don't seem to target SST INs (left panel, Mann-Whitney U ranksum test, $p=0.0115$).

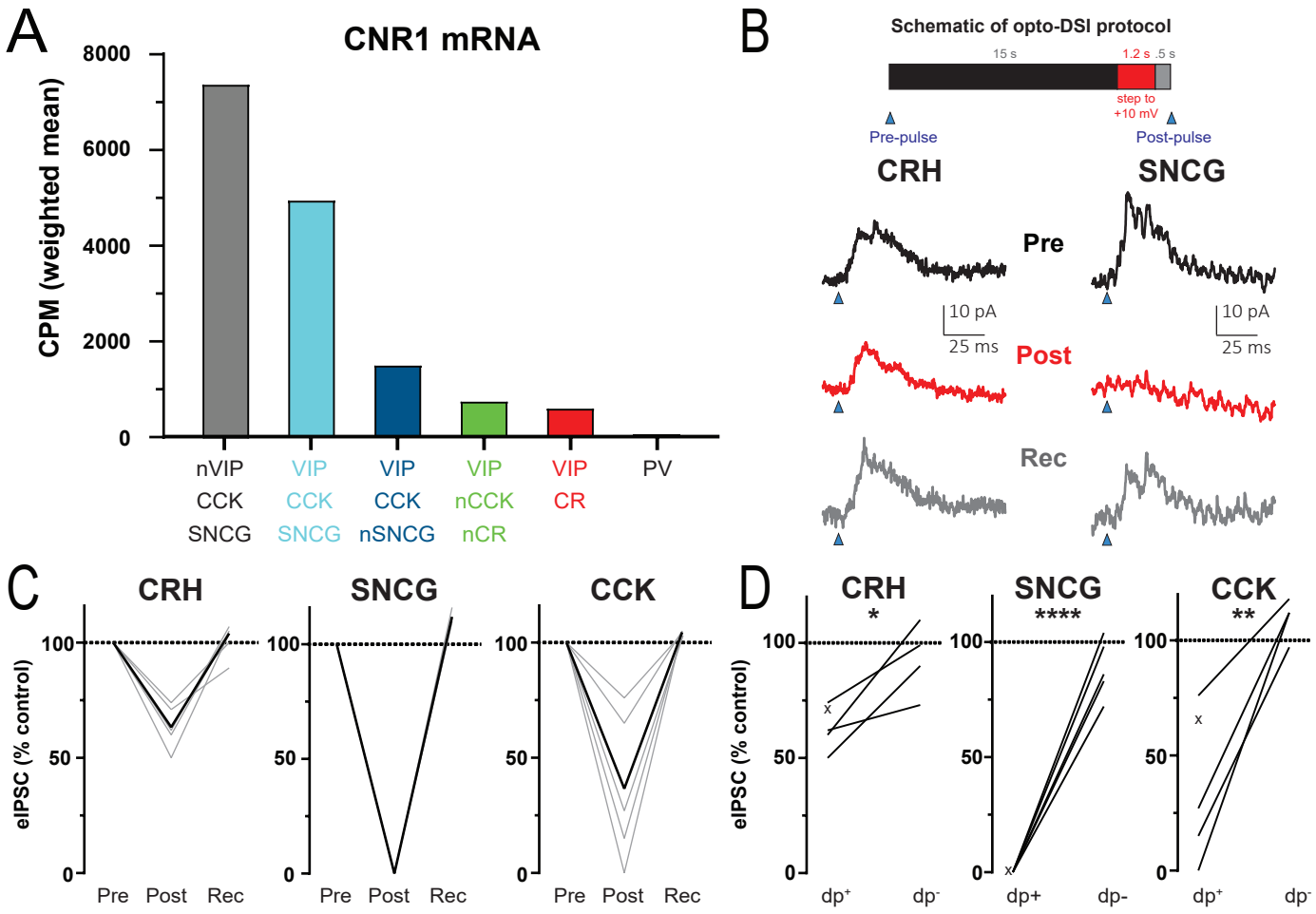

Figure 5 DSI of eIPSCs evoked by VIP INs in L2/3 PCs

A) Stacked bar plots of normalized mRNA levels (CPM weighted mean, the mean of all CPM values from all transcriptomic bins for the indicated IN subtype weighted by the number of cells in each transcriptomic bin) from the Allen Institute library for cannabinoid receptor 1 (CNR1) (Allen Institute scRNAseq data;(Yao et al., 2021)) in different VIP IN populations and PV neurons. **B)** Protocol used study depolarization-induced suppression of inhibition (DSI) (top). DSI was assessed using optogenetics in L2/3 pyramidal cells (PCs) as follows: PCs were recorded in voltage-clamp mode (V_{hold} = -50 mV) in cortical slices from VIP-Flpo/CRH;Ai80, VIP-Cre/SNCG-Flpo;Ai80 or VIP-Flpo/CCK-Cre;Ai80 mice, in which the CatCh is expressed in the intersected VIP IN subpopulation. Control IPSCs were elicited by light pulses of 2 ms in duration. Then, after a 15 s interval, the PC was depolarized (dp) to +10 mV (from -70 mV) for 1.2 s, and after a 0.5 s recovery, another IPSC was elicited by light stimulation. Averaged traces (n=3) from single cells of pre-DSI (black; top), post-DSI (red; middle), and recovery (bottom; grey) from VIP/CRH (left) and VIP/SNCG (right) Ai80 mice. **C)** DSI of all cells tested with responses normalized to the pre-depolarization step. Light, dark average of all cells (CRH, n=5; SNCG, n=6; CCK, n=5; Wilcoxon matched-pairs signed rank test, one-tailed, post vs pre, CRH, p=0.0312, SNCG, p=.0156, CCK, p=.0312). The magnitude of DSI observed in SNCG was significantly greater than that observed in CRH (Kruskal-Wallis test, p=0.002 followed by a Dunn-Sidak post-hoc test, SNCG vs. CRH, p=0.0071, SNCG vs. CCK, p=0.0894, CRH vs. CCK, p>0.9999), **D)** Summary of all cells, comparing for each cell, the effect of withholding the depolarization step (dp^+ vs dp^-, Wilcoxon matched-pairs signed rank test, one-tailed, SNCG, p=0.0312; Paired t-test, one-tailed, CRH, p=0.0173, CCK, p=0.0057) . Cells in which no dp- protocol was run are denoted by an ‘x’.

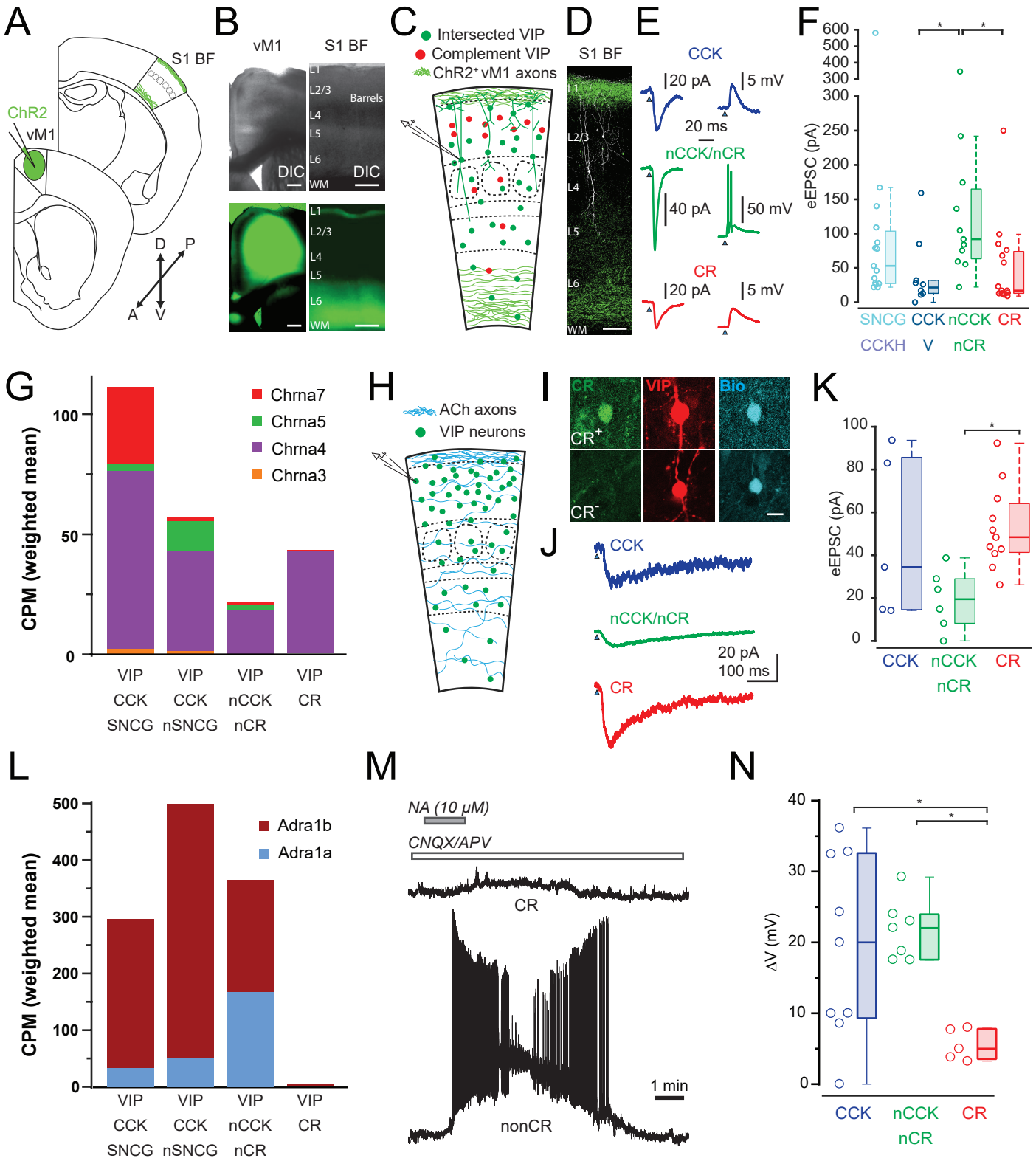

Figure 6 Differential inputs to VIP IN populations.

A) Schematic representation of the experimental procedure to study vM1 inputs onto L2-4 VIP INs in wS1, showing the injection of AAV-ChR2-EYFP into vM1, leading to the expression of ChR2 in vM1 axons projecting to Layer 1 and Layer 6 of wS1. **B)** Differential interference contrast (DIC) (top panels) and epifluorescence images (bottom panels) of the vM1 injection site (left) and the projection/recording site in wS1 (right), illustrating the ChR2- EYFP injection site and the vM1 axons in wS1. Scale bar = 200 µm. **C)** Schematic of the electrophysiological experiment in FLTG mice with the exception of VIP-Cre;SNCG-Flp;Ai65, where different VIP INs populations in wS1 were patched to measure input from L1-projecting vM1 axons upon light stimulation. **D)** Confocal image showing two patched VIP neurons, with a VIP/CR neuron (left, white) and a VIP/CCK neuron (right, white), both receiving vM1 input from L1-projecting axons (green top). Scale bar = 200 µm. **E)** Representative voltage-clamp (left, V-clamp, V_hold = -90 mV) and current-clamp (right, I-clamp) recordings from the same cells of vM1 evoked synaptic input to VIP/CCK (blue), VIP/nCCK nCR (green), and VIP/CR (red) neurons. **F)** Quantification of vM1 evoked excitatory postsynaptic currents (eEPSCs) in different VIP IN populations (SNCG+CCK H N=15, CCK V N=10, nonCCK nonCR N=11, CR N=15). Box-and-whisker plots the box represents the interquartile range (IQR: 25th to 75th percentile), the horizontal line within the box indicates the median, and whiskers extend to 1.5x the IQR unless outliers are present. Outliers are plotted individually as separate points. The stronger vM1 response was evoked in nCCK nCR VIP INs and was significantly stronger than VIP/CCK V and VIP/CR (Kruskal-Wallis p = 0.042, Dunn-Sidak nCCK nCR vs CCK V p = 0.0166 and nCCK nCR vs CR p = 0.0191). The VIP/SNCG group received the second strongest input and was not significantly different from the rest of the groups (SNCG vs CCK V p = 0.2037, SNCG vs nCCK nCR p = 0.8228, SNCG vs CR p = 0.2682) and the least responsive were VIP/CCK V and VIP/CR (CCK V vs CR p = 0.9997). **G)** Stacked bar plots of normalized mRNA levels (CPM weighted mean, the mean of all CPM values from all transcriptomic bins for the indicated IN subtype weighted by the number of cells in each transcriptomic bin; Allen Institute scRNAseq data;(Yao et al., 2021)) for nicotinic cholinergic receptor subunits (Chrna3, Chrna4, Chrna5, Chrna7) across four VIP IN populations (VIP/CCK SNCG, VIP/CCK nSNCG, VIP/nCCK nCR, and VIP/CR) showing that although all VIP populations express α nicotinic receptor subunits the VIP/nCCK nCR expresses the least. **H)** Schematic of the cholinergic input experiment, where L2-4 VIP INs were patched in a Cholinergic/VIP mouse model (ChAT-ires-Flpo; VIP-Cre; Ai80F + Cre-dependent tdTomato virus to label all VIP INs) in Layer 2/3, measuring cholinergic light-evoked currents in the presence of synaptic blockers (Gabazine and CNQX 10 µM; D-AP5 25 µM). Soma location, morphology, electrophysiological properties, and CR immunohistochemistry were used for VIP IN classification. **I)** Post hoc immunohistochemistry in brain slices showing biocytin-filled patched neurons. The images show CR+ (top) and CR- (bottom) neurons, co-labeled with VIP (red) and Biocytin (blue). Scale bar = 10 µm. **J)** Representative voltage-clamp (V-clamp) recordings of cholinergic light-evoked currents in VIP/CCK (blue), VIP/nCCK nCR (green), and VIP/CR (red) neurons. **K)** Quantification of cholinergic input (eEPSCs) to VIP neurons (CCK, N=5, nCCK nCR N=6, CR N=11, Kruskal-Wallis test p=0.0127, Dunn-Sidak CCK vs nCCK nCR p=0.3129, CCK vs CR p>0.9999, nCCK nCR vs CR p=0.0147). **L)** Stacked bar plots of normalized mRNA levels (CPM weighted mean as in

G; Allen Institute scRNAseq data;(Yao et al., 2021)) for α1-adrenergic receptor subunits (Adra1a, Adra1b) across the four VIP interneuron subpopulations (VIP/CCK SNCG, VIP/CCK nSNCG, VIP/nCCK nCR, VIP/ CR). The height of each colored segment represents the relative contribution of each subunit to the total expression. **M)** Representative traces of noradrenaline (NA, 10 μM) application in the presence of glutamate blockers, showing differential effects in a VIP/CR vs. a VIP/nonCR neuron The VIP/CR neuron exhibited a modest membrane potential depolarization, whereas the VIP/nonCR neuron showed a strong depolarization with spiking. **N)** Quantification of membrane potential change (ΔV, if cell began spiking than spiking threshold was used as the final Vm reached) after NA application demonstrating a significantly greater NA-induced depolarization in VIP/CCK and VIP/nCCK nCR neurons, with many reaching spiking threshold, compared to VIP/CR neurons (CCK, N=9, nCCK nCR N=7, CR N=5, Kruskal-Wallis test p=0.0091, Dunn-Sidak CCK vs nCCK nCR p>0.9999, CCK vs CR p=0.0336, nCCK nCR vs CR p=0.0225).

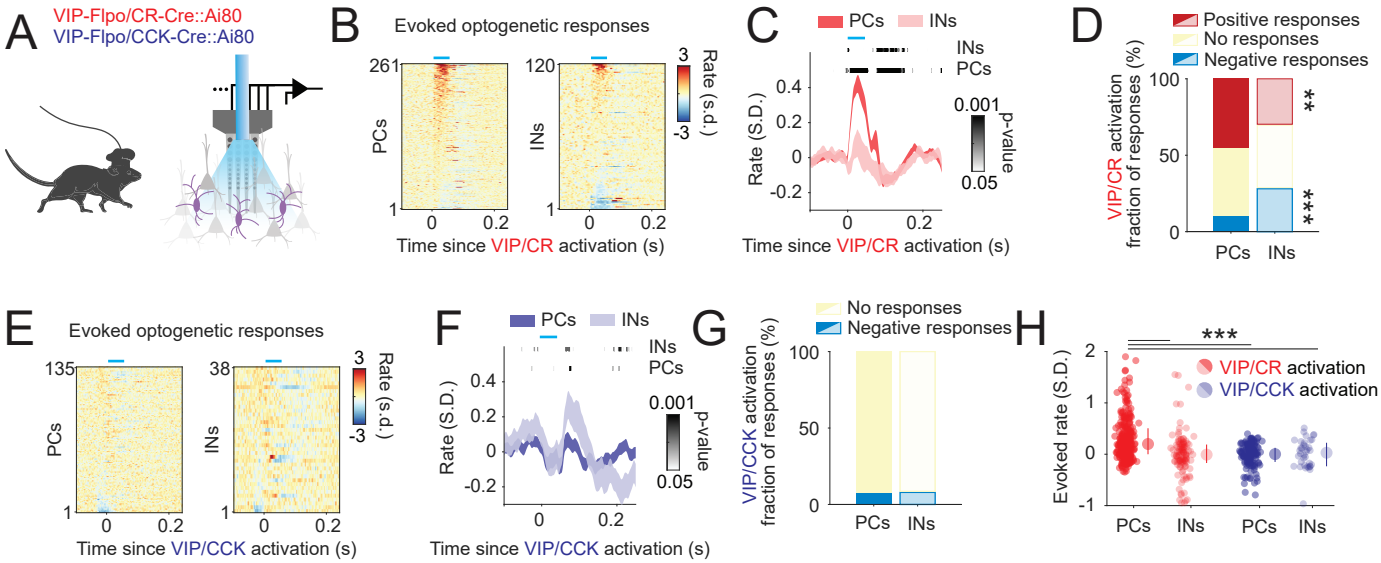

Figure 7 Network effects of the activation of VIP/CR and VIP/CCK INs.

(A) Optogenetic activation of VIP/CR and VIP/CCK neurons in freely behaving mice. Combined optical fiber-electrode probes were implanted in VIP-Flpo/CR-Cre::Ai80 and VIP-Flpo/CCK-Cre::Ai80 mice to enable simultaneous stimulation and recording. **(B)** Peristimulus time histograms (PSTHs) of pyramidal cells and interneurons in the posterior parietal cortex (PTLp) following VIP/CR IN activation, sorted by light stimulus (n = 4 mice). **(C)** Average firing rate (± s.d.) peri-stimulus time histograms (PSTHs) for pyramidal cells and interneurons. The significance of the average response in each spatial bin was assessed using the Wilcoxon rank test and is shown for both groups. **(D)** Fraction of positive, negative, and non-significant responses (bootstrap, 1000 repetitions) following VIP/CR IN activation across groups. A higher fraction of pyramidal cells was ontogenetically disinhibited by VIP/CR activation (45.2% vs. 30.0%, $p = 0.005$, Chi-square test). Conversely, a greater fraction of interneurons was suppressed by the same manipulation (10.3% vs. 28.3%, $p < 10^{-5}$). **(E-F)** Same as in B-C for VIP/CCK IN activation (n = 2 mice). **(G)** A comparable fraction of pyramidal cells and interneurons was suppressed by VIP/CCK IN activation (7.4% and 7.8%, p = 0.95). **(H)** Pyramidal cells were disinhibited by optogenetic activation of VIP/CR INs (two-way ANOVA: effect of optogenetically activated cell group, $F_{1,549} = 16.5$, $p < 10^{-4}$; effect of response group, $F_{1,549} = 8.2$, p = 0.004; interaction between activated and response groups, $F_{1,549} = 11.8$, $p < 10^{-3}$).

Acknowledgments

We thank Chiung-Yin Chung for all her assistance; Maximiliano Jose Nigro, Brian Clark, Sebnem Tuncdemir, and Robin Tremblay for their data to train the PV/SST classifier; Benjamin Schuman and Bryce Grier for their helpful discussions and guidance; this work was supported by NIH grants R01NS133751, R21MH137452, and P01NS074972.

References

Acsady, L., Arabadzisz, D., & Freund, T. F. (1996). Correlated morphological and neurochemical features identify different subsets of vasoactive intestinal polypeptide-immunoreactive interneurons in rat hippocampus. *Neuroscience*, *73*(2), 299-315. https://doi.org/10.1016/0306-4522(95)00610-9

Acsady, L., Gorcs, T. J., & Freund, T. F. (1996). Different populations of vasoactive intestinal polypeptide-immunoreactive interneurons are specialized to control pyramidal cells or interneurons in the hippocampus. *Neuroscience*, *73*(2), 317-334. https://doi.org/10.1016/0306-4522(95)00609-5

Apicella, A. J., & Marchionni, I. (2022). VIP-Expressing GABAergic Neurons: Disinhibitory vs. Inhibitory Motif and Its Role in Communication Across Neocortical Areas. *Front Cell Neurosci*, *16*, 811484. https://doi.org/10.3389/fncel.2022.811484

Askew, C. E., Lopez, A. J., Wood, M. A., & Metherate, R. (2019). Nicotine excites VIP interneurons to disinhibit pyramidal neurons in auditory cortex. *Synapse*, *73*(9), e22116. https://doi.org/10.1002/syn.22116

Batista-Brito, R., Vinck, M., Ferguson, K. A., Chang, J. T., Laubender, D., Lur, G., Mossner, J. M., Hernandez, V. G., Ramakrishnan, C., Deisseroth, K., Higley, M. J., & Cardin, J. A. (2017). Developmental Dysfunction of VIP Interneurons Impairs Cortical Circuits. *Neuron*, *95*(4), 884-895 e889. https://doi.org/10.1016/j.neuron.2017.07.034

Bigelow, J., Morrill, R. J., Dekloe, J., & Hasenstaub, A. R. (2019). Movement and VIP Interneuron Activation Differentially Modulate Encoding in Mouse Auditory Cortex. *eNeuro*, *6*(5). https://doi.org/10.1523/ENEURO.0164-19.2019

Bodor, A. L., Katona, I., Nyiri, G., Mackie, K., Ledent, C., Hajos, N., & Freund, T. F. (2005). Endocannabinoid signaling in rat somatosensory cortex: laminar differences and involvement of specific interneuron types. *J Neurosci*, *25*(29), 6845-6856. https://doi.org/10.1523/JNEUROSCI.0442-05.2005

Canto-Bustos, M., Friason, F. K., Bassi, C., & Oswald, A. M. (2022). Disinhibitory Circuitry Gates Associative Synaptic Plasticity in Olfactory Cortex. *J Neurosci*, *42*(14), 2942-2950. https://doi.org/10.1523/JNEUROSCI.1369-21.2021

Cauli, B., Porter, J. T., Tsuzuki, K., Lambolez, B., Rossier, J., Quenet, B., & Audinat, E. (2000). Classification of fusiform neocortical interneurons based on unsupervised clustering. *Proc Natl Acad Sci U S A*, *97*(11), 6144-6149. https://doi.org/10.1073/pnas.97.11.6144

Daigle, T. L., Madisen, L., Hage, T. A., Valley, M. T., Knoblich, U., Larsen, R. S., Takeno, M. M., Huang, L., Gu, H., Larsen, R., Mills, M., Bosma-Moody, A., Siverts, L. A., Walker, M., Graybuck, L. T., Yao, Z., Fong, O., Nguyen, T. N., Garren, E.,…Zeng, H. (2018). A Suite of Transgenic Driver and Reporter Mouse Lines with Enhanced Brain-Cell-Type Targeting and Functionality. *Cell*, *174*(2), 465-480 e422. https://doi.org/10.1016/j.cell.2018.06.035

DeFelipe, J. (2002). Cortical interneurons: from Cajal to 2001. *Prog Brain Res*, *136*, 215-238. https://doi.org/10.1016/s0079-6123(02)36019-9

Dudok, B., Klein, P. M., Hwaun, E., Lee, B. R., Yao, Z., Fong, O., Bowler, J. C., Terada, S., Sparks, F. T., Szabo, G. G., Farrell, J. S., Berg, J., Daigle, T. L., Tasic, B.,

Dimidschstein, J., Fishell, G., Losonczy, A., Zeng, H., & Soltesz, I. (2021). Alternating sources of perisomatic inhibition during behavior. *Neuron*, *109*(6), 997-1012 e1019. https://doi.org/10.1016/j.neuron.2021.01.003

Fishell, G., & Kepecs, A. (2020). Interneuron Types as Attractors and Controllers. *Annu Rev Neurosci*, *43*, 1-30. https://doi.org/10.1146/annurev-neuro-070918-050421

Freund, T. F., Magloczky, Z., Soltesz, I., & Somogyi, P. (1986). Synaptic connections, axonal and dendritic patterns of neurons immunoreactive for cholecystokinin in the visual cortex of the cat. *Neuroscience*, *19*(4), 1133-1159. https://doi.org/10.1016/0306-4522(86)90129-6

Fu, Y., Kaneko, M., Tang, Y., Alvarez-Buylla, A., & Stryker, M. P. (2015). A cortical disinhibitory circuit for enhancing adult plasticity. *Elife*, *4*, e05558. https://doi.org/10.7554/eLife.05558

Fu, Y., Tucciarone, J. M., Espinosa, J. S., Sheng, N., Darcy, D. P., Nicoll, R. A., Huang, Z. J., & Stryker, M. P. (2014). A cortical circuit for gain control by behavioral state. *Cell*, *156*(6), 1139-1152. https://doi.org/10.1016/j.cell.2014.01.050

Furlanis, E., Dai, M., Leyva Garcia, B., Vergara, J., Pereira, A., Pelkey, K., Tran, T., Gorissen, B. L., Vlachos, A., Hairston, A., Huang, S., Dwivedi, D., Du, S., Wills, S., McMahon, J., Lee, A. T., Chang, E. F., Razzaq, T., Qazi, A.,…Wang, Y. (2024). An enhancer-AAV toolbox to target and manipulate distinct interneuron subtypes. *bioRxiv*. https://doi.org/10.1101/2024.07.17.603924

Galarreta, M., Erdelyi, F., Szabo, G., & Hestrin, S. (2008). Cannabinoid sensitivity and synaptic properties of 2 GABAergic networks in the neocortex. *Cereb Cortex*, *18*(10), 2296-2305. https://doi.org/10.1093/cercor/bhm253

Gasselin, C., Hohl, B., Vernet, A., Crochet, S., & Petersen, C. C. H. (2021). Cell-type-specific nicotinic input disinhibits mouse barrel cortex during active sensing. *Neuron*, *109*(5), 778-787 e773. https://doi.org/10.1016/j.neuron.2020.12.018

Gentet, L. J., Kremer, Y., Taniguchi, H., Huang, Z. J., Staiger, J. F., & Petersen, C. C. (2012). Unique functional properties of somatostatin-expressing GABAergic neurons in mouse barrel cortex. *Nat Neurosci*, *15*(4), 607-612. https://doi.org/10.1038/nn.3051

Goff, K. M., & Goldberg, E. M. (2019). Vasoactive intestinal peptide-expressing interneurons are impaired in a mouse model of Dravet syndrome. *Elife*, *8*. https://doi.org/10.7554/eLife.46846

Goff, K. M., Liebergall, S. R., Jiang, E., Somarowthu, A., & Goldberg, E. M. (2023). VIP interneuron impairment promotes in vivo circuit dysfunction and autism-related behaviors in Dravet syndrome. *Cell Rep*, *42*(6), 112628. https://doi.org/10.1016/j.celrep.2023.112628

Goldberg, E. M., Jeong, H. Y., Kruglikov, I., Tremblay, R., Lazarenko, R. M., & Rudy, B. (2011). Rapid developmental maturation of neocortical FS cell intrinsic excitability. *Cereb Cortex*, *21*(3), 666-682. https://doi.org/10.1093/cercor/bhq138

Gonchar, Y., & Burkhalter, A. (2003). Distinct GABAergic targets of feedforward and feedback connections between lower and higher areas of rat visual cortex. *J Neurosci*, *23*(34), 10904-10912. https://www.ncbi.nlm.nih.gov/pubmed/14645486

Gouwens, N. W., Sorensen, S. A., Baftizadeh, F., Budzillo, A., Lee, B. R., Jarsky, T., Alfiler, L., Baker, K., Barkan, E., Berry, K., Bertagnolli, D., Bickley, K., Bomben, J., Braun, T., Brouner, K., Casper, T., Crichton, K., Daigle, T. L.,

Dalley, R.,…Zeng, H. (2020). Integrated Morphoelectric and Transcriptomic Classification of Cortical GABAergic Cells. *Cell*, *183*(4), 935-953 e919. https://doi.org/10.1016/j.cell.2020.09.057

Green, J., Bruno, C. A., Traunmuller, L., Ding, J., Hrvatin, S., Wilson, D. E., Khodadad, T., Samuels, J., Greenberg, M. E., & Harvey, C. D. (2023). A cell-type-specific error-correction signal in the posterior parietal cortex. *Nature*, *620*(7973), 366-373. https://doi.org/10.1038/s41586-023-06357-1

Gulyas, A. I., Hajos, N., & Freund, T. F. (1996). Interneurons containing calretinin are specialized to control other interneurons in the rat hippocampus. *J Neurosci*, *16*(10), 3397-3411. https://www.ncbi.nlm.nih.gov/pubmed/8627375

Hajos, N., Acsady, L., & Freund, T. F. (1996). Target selectivity and neurochemical characteristics of VIP-immunoreactive interneurons in the rat dentate gyrus. *Eur J Neurosci*, *8*(7), 1415-1431. https://doi.org/10.1111/j.1460-9568.1996.tb01604.x

He, M., Tucciarone, J., Lee, S., Nigro, M. J., Kim, Y., Levine, J. M., Kelly, S. M., Krugikov, I., Wu, P., Chen, Y., Gong, L., Hou, Y., Osten, P., Rudy, B., & Huang, Z. J. (2016). Strategies and Tools for Combinatorial Targeting of GABAergic Neurons in Mouse Cerebral Cortex. *Neuron*, *91*(6), 1228-1243. https://doi.org/10.1016/j.neuron.2016.08.021

Hostetler, R. E., Hu, H., & Agmon, A. (2023). Genetically Defined Subtypes of Somatostatin-Containing Cortical Interneurons. *eNeuro*, *10*(8), ENEURO.0204-0223.2023. https://doi.org/10.1523/ENEURO.0204-23.2023

Hrvatin, S., Tzeng, C. P., Nagy, M. A., Stroud, H., Koutsioumpa, C., Wilcox, O. F., Assad, E. G., Green, J., Harvey, C. D., Griffith, E. C., & Greenberg, M. E. (2019). A scalable platform for the development of cell-type-specific viral drivers. *Elife*, *8*, e48089. https://doi.org/10.7554/eLife.48089

Jiang, X., Shen, S., Cadwell, C. R., Berens, P., Sinz, F., Ecker, A. S., Patel, S., & Tolias, A. S. (2015). Principles of connectivity among morphologically defined cell types in adult neocortex. *Science*, *350*(6264), aac9462. https://doi.org/10.1126/science.aac9462

Jiang, X., Wang, G., Lee, A. J., Stornetta, R. L., & Zhu, J. J. (2013). The organization of two new cortical interneuronal circuits. *Nat Neurosci*, *16*(2), 210-218. https://doi.org/10.1038/nn.3305

Kawaguchi, Y., & Kubota, Y. (1996). Physiological and morphological identification of somatostatin- or vasoactive intestinal polypeptide-containing cells among GABAergic cell subtypes in rat frontal cortex. *J Neurosci*, *16*(8), 2701-2715. https://www.ncbi.nlm.nih.gov/pubmed/8786446

Kawaguchi, Y., & Kubota, Y. (1998). Neurochemical features and synaptic connections of large physiologically-identified GABAergic cells in the rat frontal cortex. *Neuroscience*, *85*(3), 677-701. https://doi.org/10.1016/s0306-4522(97)00685-4

Koukouli, F., Rooy, M., Tziotis, D., Sailor, K. A., O'Neill, H. C., Levenga, J., Witte, M., Nilges, M., Changeux, J. P., Hoeffer, C. A., Stitzel, J. A., Gutkin, B. S., DiGregorio, D. A., & Maskos, U. (2017). Nicotine reverses hypofrontality in animal models of addiction and schizophrenia. *Nat Med*, *23*(3), 347-354. https://doi.org/10.1038/nm.4274

Kubota, Y. (2014). Untangling GABAergic wiring in the cortical microcircuit. *Curr Opin Neurobiol*, *26*, 7-14. https://doi.org/10.1016/j.conb.2013.10.003

Kullander, K., & Topolnik, L. (2021). Cortical disinhibitory circuits: cell types, connectivity and function. *Trends Neurosci*, *44*(8), 643-657. https://doi.org/10.1016/j.tins.2021.04.009

Lee, A. T., Cunniff, M. M., See, J. Z., Wilke, S. A., Luongo, F. J., Ellwood, I. T., Ponnavolu, S., & Sohal, V. S. (2019). VIP Interneurons Contribute to Avoidance Behavior by Regulating Information Flow across Hippocampal-Prefrontal Networks. *Neuron*, *102*(6), 1223-1234 e1224. https://doi.org/10.1016/j.neuron.2019.04.001

Lee, S., Hjerling-Leffler, J., Zagha, E., Fishell, G., & Rudy, B. (2010). The largest group of superficial neocortical GABAergic interneurons expresses ionotropic serotonin receptors. *J Neurosci*, *30*(50), 16796-16808. https://doi.org/10.1523/JNEUROSCI.1869-10.2010

Lee, S., Kruglikov, I., Huang, Z. J., Fishell, G., & Rudy, B. (2013). A disinhibitory circuit mediates motor integration in the somatosensory cortex. *Nat Neurosci*, *16*(11), 1662-1670. https://doi.org/10.1038/nn.3544

Letzkus, J. J., Wolff, S. B., & Luthi, A. (2015). Disinhibition, a Circuit Mechanism for Associative Learning and Memory. *Neuron*, *88*(2), 264-276. https://doi.org/10.1016/j.neuron.2015.09.024

Letzkus, J. J., Wolff, S. B., Meyer, E. M., Tovote, P., Courtin, J., Herry, C., & Luthi, A. (2011). A disinhibitory microcircuit for associative fear learning in the auditory cortex. *Nature*, *480*(7377), 331-335. https://doi.org/10.1038/nature10674

Liodis, P., Denaxa, M., Grigoriou, M., Akufo-Addo, C., Yanagawa, Y., & Pachnis, V. (2007). Lhx6 activity is required for the normal migration and specification of cortical interneuron subtypes. *J Neurosci*, *27*(12), 3078-3089. https://doi.org/10.1523/JNEUROSCI.3055-06.2007

Ma, Y., Hu, H., Berrebi, A. S., Mathers, P. H., & Agmon, A. (2006). Distinct subtypes of somatostatin-containing neocortical interneurons revealed in transgenic mice. *J Neurosci*, *26*(19), 5069-5082. https://doi.org/10.1523/JNEUROSCI.0661-06.2006

Machold, R., Dellal, S., Valero, M., Zurita, H., Kruglikov, I., Meng, J. H., Hanson, J. L., Hashikawa, Y., Schuman, B., Buzsaki, G., & Rudy, B. (2023). Id2 GABAergic interneurons comprise a neglected fourth major group of cortical inhibitory cells. *Elife*, *12*, e85893. https://doi.org/10.7554/eLife.85893

Machold, R., & Rudy, B. (2024). Genetic approaches to elucidating cortical and hippocampal GABAergic interneuron diversity. *Front Cell Neurosci*, *18*, 1414955. https://doi.org/10.3389/fncel.2024.1414955

Melzer, S., Newmark, E. R., Mizuno, G. O., Hyun, M., Philson, A. C., Quiroli, E., Righetti, B., Gregory, M. R., Huang, K. W., Levasseur, J., Tian, L., & Sabatini, B. L. (2021). Bombesin-like peptide recruits disinhibitory cortical circuits and enhances fear memories. *Cell*, *184*(22), 5622-5634 e5625. https://doi.org/10.1016/j.cell.2021.09.013

Meng, J. H. K., Yijie; Li, Alan; Feyerabend, Michael; Inoue, Wataru; Martinez-Trujillo, Julio; Rudy, Bernardo; Wang, Xiao-Jing. (2024). In Search of Transcriptomic Correlates of Neuronal Firing-Rate Adaptation across Subtypes, Regions and Species: A Patch-seq Analysis. *bioRxiv*. https://doi.org/10.1101/2024.12.05.627057

Mossner, J. M., Batista-Brito, R., Pant, R., & Cardin, J. A. (2020). Developmental loss of MeCP2 from VIP interneurons impairs cortical function and behavior. *Elife*, *9*. https://doi.org/10.7554/eLife.55639

Muñoz, W., Tremblay, R., Levenstein, D., & Rudy, B. (2017). Layer-specific modulation of neocortical dendritic inhibition during active wakefulness. *Science*, *355*(6328), 954-959. https://doi.org/10.1126/science.aag2599

Naskar, S., Qi, J., Pereira, F., Gerfen, C. R., & Lee, S. (2021). Cell-type-specific recruitment of GABAergic interneurons in the primary somatosensory cortex by long-range inputs. *Cell Rep*, *34*(8), 108774. https://doi.org/10.1016/j.celrep.2021.108774

Nigro, M. J., Hashikawa-Yamasaki, Y., & Rudy, B. (2018). Diversity and Connectivity of Layer 5 Somatostatin-Expressing Interneurons in the Mouse Barrel Cortex. *J Neurosci*, *38*(7), 1622-1633. https://doi.org/10.1523/JNEUROSCI.2415-17.2017

Ohno-Shosaku, T., Maejima, T., & Kano, M. (2001). Endogenous cannabinoids mediate retrograde signals from depolarized postsynaptic neurons to presynaptic terminals. *Neuron*, *29*(3), 729-738. https://doi.org/10.1016/s0896-6273(01)00247-1

Petersen, P. C. (2019). *phy-plugins (Version 1.0)*. In https://github.com/petersenpeter/phy-plugins

Petersen, P. C., Watson, B., & Peyrache, A. (2020). *KiloSortWrapper (Version 1.0)*. In Zenodo. https://doi.org/10.5281/zenodo.3604165

Pfeffer, C. K., Xue, M., He, M., Huang, Z. J., & Scanziani, M. (2013). Inhibition of inhibition in visual cortex: the logic of connections between molecularly distinct interneurons. *Nat Neurosci*, *16*(8), 1068-1076. https://doi.org/10.1038/nn.3446

Pi, H. J., Hangya, B., Kvitsiani, D., Sanders, J. I., Huang, Z. J., & Kepecs, A. (2013). Cortical interneurons that specialize in disinhibitory control. *Nature*, *503*(7477), 521-524. https://doi.org/10.1038/nature12676

Pitler, T. A., & Alger, B. E. (1992). Postsynaptic spike firing reduces synaptic GABAA responses in hippocampal pyramidal cells. *J Neurosci*, *12*(10), 4122-4132. https://doi.org/10.1523/JNEUROSCI.12-10-04122.1992

Plummer, N. W., Evsyukova, I. Y., Robertson, S. D., de Marchena, J., Tucker, C. J., & Jensen, P. (2015). Expanding the power of recombinase-based labeling to uncover cellular diversity. *Development*, *142*(24), 4385-4393. https://doi.org/10.1242/dev.129981

Porter, J. T., Cauli, B., Staiger, J. F., Lambolez, B., Rossier, J., & Audinat, E. (1998). Properties of bipolar VIPergic interneurons and their excitation by pyramidal neurons in the rat neocortex. *Eur J Neurosci*, *10*(12), 3617-3628. https://doi.org/10.1046/j.1460-9568.1998.00367.x

Pronneke, A., Scheuer, B., Wagener, R. J., Mock, M., Witte, M., & Staiger, J. F. (2015). Characterizing VIP Neurons in the Barrel Cortex of VIPcre/tdTomato Mice Reveals Layer-Specific Differences. *Cereb Cortex*, *25*(12), 4854-4868. https://doi.org/10.1093/cercor/bhv202

Pronneke, A., Witte, M., Mock, M., & Staiger, J. F. (2020). Neuromodulation Leads to a Burst-Tonic Switch in a Subset of VIP Neurons in Mouse Primary Somatosensory (Barrel) Cortex. *Cereb Cortex*, *30*(2), 488-504. https://doi.org/10.1093/cercor/bhz102

Ramón y Cajal, S. (1911). *Histologie du système nerveux de l'homme et des vertébrés* (Édition française revue et mise à jour par l'auteur, traduite de l'espagnol par L. Azoulay ed., Vol. 2). A. Maloine.

Ramos-Prats, A., Paradiso, E., Castaldi, F., Sadeghi, M., Mir, M. Y., Hortnagl, H., Gobel, G., & Ferraguti, F. (2022). VIP-expressing interneurons in the anterior insular cortex contribute to sensory processing to regulate adaptive behavior. *Cell Rep*, *39*(9), 110893. https://doi.org/10.1016/j.celrep.2022.110893

Rossant, C. (2021). *Phy 2 (Version 2.0)*. In https://github.com/kwikteam/phy

Sachidhanandam, S., Sermet, B. S., & Petersen, C. C. H. (2016). Parvalbumin-Expressing GABAergic Neurons in Mouse Barrel Cortex Contribute to Gating a Goal-Directed Sensorimotor Transformation. *Cell Rep*, *15*(4), 700-706. https://doi.org/10.1016/j.celrep.2016.03.063

Schuman, B., Dellal, S., Pronneke, A., Machold, R., & Rudy, B. (2021). Neocortical Layer 1: An Elegant Solution to Top-Down and Bottom-Up Integration. *Annu Rev Neurosci*, *44*, 221-252. https://doi.org/10.1146/annurev-neuro-100520-012117

Senzai, Y., Fernandez-Ruiz, A., & Buzsaki, G. (2019). Layer-Specific Physiological Features and Interlaminar Interactions in the Primary Visual Cortex of the Mouse. *Neuron*, *101*(3), 500-513 e505. https://doi.org/10.1016/j.neuron.2018.12.009

Taniguchi, H., He, M., Wu, P., Kim, S., Paik, R., Sugino, K., Kvitsiani, D., Fu, Y., Lu, J., Lin, Y., Miyoshi, G., Shima, Y., Fishell, G., Nelson, S. B., & Huang, Z. J. (2011). A resource of Cre driver lines for genetic targeting of GABAergic neurons in cerebral cortex. *Neuron*, *71*(6), 995-1013. https://doi.org/10.1016/j.neuron.2011.07.026

Tasic, B., Menon, V., Nguyen, T. N., Kim, T. K., Jarsky, T., Yao, Z., Levi, B., Gray, L. T., Sorensen, S. A., Dolbeare, T., Bertagnolli, D., Goldy, J., Shapovalova, N., Parry, S., Lee, C., Smith, K., Bernard, A., Madisen, L., Sunkin, S. M.,…Zeng, H. (2016). Adult mouse cortical cell taxonomy revealed by single cell transcriptomics. *Nat Neurosci*, *19*(2), 335-346. https://doi.org/10.1038/nn.4216

Tasic, B., Yao, Z., Graybuck, L. T., Smith, K. A., Nguyen, T. N., Bertagnolli, D., Goldy, J., Garren, E., Economo, M. N., Viswanathan, S., Penn, O., Bakken, T., Menon, V., Miller, J., Fong, O., Hirokawa, K. E., Lathia, K., Rimorin, C., Tieu, M.,…Zeng, H. (2018). Shared and distinct transcriptomic cell types across neocortical areas. *Nature*, *563*(7729), 72-78. https://doi.org/10.1038/s41586-018-0654-5

Topolnik, L., & Tamboli, S. (2022). The role of inhibitory circuits in hippocampal memory processing. *Nat Rev Neurosci*, *23*(8), 476-492. https://doi.org/10.1038/s41583-022-00599-0

Tremblay, R., Lee, S., & Rudy, B. (2016). GABAergic Interneurons in the Neocortex: From Cellular Properties to Circuits. *Neuron*, *91*(2), 260-292. https://doi.org/10.1016/j.neuron.2016.06.033

Turi, G. F., Li, W. K., Chavlis, S., Pandi, I., O'Hare, J., Priestley, J. B., Grosmark, A. D., Liao, Z., Ladow, M., Zhang, J. F., Zemelman, B. V., Poirazi, P., & Losonczy, A. (2019). Vasoactive Intestinal Polypeptide-Expressing Interneurons in the Hippocampus Support Goal-Oriented Spatial Learning. *Neuron*, *101*(6), 1150-1165 e1158. https://doi.org/10.1016/j.neuron.2019.01.009

Tyan, L., Chamberland, S., Magnin, E., Camire, O., Francavilla, R., David, L. S., Deisseroth, K., & Topolnik, L. (2014). Dendritic inhibition provided by interneuron-specific cells controls the firing rate and timing of the hippocampal feedback inhibitory circuitry. *J Neurosci*, *34*(13), 4534-4547. https://doi.org/10.1523/JNEUROSCI.3813-13.2014

Valero, M., Navas-Olive, A., de la Prida, L. M., & Buzsaki, G. (2022). Inhibitory conductance controls place field dynamics in the hippocampus. *Cell Rep*, *40*(8), 111232. https://doi.org/10.1016/j.celrep.2022.111232

Valero, M., Viney, T. J., Machold, R., Mederos, S., Zutshi, I., Schuman, B., Senzai, Y., Rudy, B., & Buzsaki, G. (2021). Sleep down state-active ID2/Nkx2.1 interneurons in the neocortex. *Nat Neurosci*, *24*(3), 401-411. https://doi.org/10.1038/s41593-021-00797-6

Vormstein-Schneider, D., Lin, J. D., Pelkey, K. A., Chittajallu, R., Guo, B., Arias-Garcia, M. A., Allaway, K., Sakopoulos, S., Schneider, G., Stevenson, O., Vergara, J., Sharma, J., Zhang, Q., Franken, T. P., Smith, J., Ibrahim, L. A., Mastro, K. J., Sabri, E., Huang, S.,…Dimidschstein, J. (2020). Viral manipulation of functionally distinct interneurons in mice, non-human primates and humans. *Nat Neurosci*, *23*(12), 1629-1636. https://doi.org/10.1038/s41593-020-0692-9

Wagner, J. J., & Alger, B. E. (1996). Increased neuronal excitability during depolarization-induced suppression of inhibition in rat hippocampus. *J Physiol*, *495 (Pt 1)*(Pt 1), 107-112. https://doi.org/10.1113/jphysiol.1996.sp021577

Wang, X., Tucciarone, J., Jiang, S., Yin, F., Wang, B. S., Wang, D., Jia, Y., Jia, X., Li, Y., Yang, T., Xu, Z., Akram, M. A., Wang, Y., Zeng, S., Ascoli, G. A., Mitra, P., Gong, H., Luo, Q., & Huang, Z. J. (2019). Genetic Single Neuron Anatomy Reveals Fine Granularity of Cortical Axo-Axonic Cells. *Cell Rep*, *26*(11), 3145-3159 e3145. https://doi.org/10.1016/j.celrep.2019.02.040

Wang, Y., Gupta, A., Toledo-Rodriguez, M., Wu, C. Z., & Markram, H. (2002). Anatomical, physiological, molecular and circuit properties of nest basket cells in the developing somatosensory cortex. *Cereb Cortex*, *12*(4), 395-410. https://doi.org/10.1093/cercor/12.4.395

Williams, L. E., & Holtmaat, A. (2019). Higher-Order Thalamocortical Inputs Gate Synaptic Long-Term Potentiation via Disinhibition. *Neuron*, *101*(1), 91-102 e104. https://doi.org/10.1016/j.neuron.2018.10.049

Wilson, R. I., Kunos, G., & Nicoll, R. A. (2001). Presynaptic specificity of endocannabinoid signaling in the hippocampus. *Neuron*, *31*(3), 453-462. https://doi.org/10.1016/s0896-6273(01)00372-5

Wilson, R. I., & Nicoll, R. A. (2001). Endogenous cannabinoids mediate retrograde signalling at hippocampal synapses. *Nature*, *410*(6828), 588-592. https://doi.org/10.1038/35069076

Wu, S. J., Sevier, E., Dwivedi, D., Saldi, G. A., Hairston, A., Yu, S., Abbott, L., Choi, D. H., Sherer, M., Qiu, Y., Shinde, A., Lenahan, M., Rizzo, D., Xu, Q., Barrera, I., Kumar, V., Marrero, G., Pronneke, A., Huang, S.,…Fishell, G. (2023). Cortical somatostatin interneuron subtypes form cell-type-specific circuits. *Neuron*, *111*(17), 2675-2692 e2679. https://doi.org/10.1016/j.neuron.2023.05.032

Yao, Z., van Velthoven, C. T. J., Nguyen, T. N., Goldy, J., Sedeno-Cortes, A. E., Baftizadeh, F., Bertagnolli, D., Casper, T., Chiang, M., Crichton, K., Ding, S. L.,

Fong, O., Garren, E., Glandon, A., Gouwens, N. W., Gray, J., Graybuck, L. T., Hawrylycz, M. J., Hirschstein, D.,…Zeng, H. (2021). A taxonomy of transcriptomic cell types across the isocortex and hippocampal formation. *Cell*, *184*(12), 3222-3241 e3226. https://doi.org/10.1016/j.cell.2021.04.021

Zhang, S., Xu, M., Kamigaki, T., Hoang Do, J. P., Chang, W. C., Jenvay, S., Miyamichi, K., Luo, L., & Dan, Y. (2014). Selective attention. Long-range and local circuits for top-down modulation of visual cortex processing. *Science*, *345*(6197), 660-665. https://doi.org/10.1126/science.1254126